January 2010

Electromagnetic Tracking for Medical Imaging

Jie Wen
Washington University in St. Louis

WASHINGTON UNIVERSITY IN ST. LOUIS

School of Engineering and Applied Science

Department of Electrical and Systems Engineering

Thesis Examination Committee:
Joseph A O'Sullivan
Barry Spielman
Lan Yang

Electromagnetic Tracking for Medical Imaging

by

Jie Wen

A thesis presented to the School of Engineering

of Washington University in partial fulfillment of the

requirements for the degree of

MASTER OF SCIENCE

MAY 2010

Saint Louis, Missouri

ABSTRACT OF THE THESIS

Electromagnetic Tracking for Medical Imaging

by

Jie Wen

Master of Science in Electrical Engineering

Washington University in St. Louis, 2010

Research Advisor: Professor Parag J. Parikh

This thesis explores the novel use of a wireless electromagnetic (EM) tracking device in a Computed Tomography (CT) environment. The sources of electromagnetic interference inside a Philips Brilliant Big Bore CT scanner are analyzed. A research version of the Calypso wireless tracking system was set up inside the CT suite, and a set of three Beacon transponders was bonded to a plastic fixture. The tracking system was tested under different working parameters including orientation of tracking beacons, the gain level of the frontend amplifier, the distance between the transponders and the sensor array, the rotation speed of the CT gantry, and the presence/absence of the CT X-ray source. The performance of the tracking system reveals two obvious factors which bring in electromagnetic interference: 1) metal like effect brought in by carbon fiber patient couch and 2) electromagnetic disturbance due to spinning metal inside the CT gantry. The accuracy requirements for electromagnetic tracking in the CT environment are a Root Mean Square (RMS) error of <2 mm in stationary position tracking. Within a working volume of $120\times120\times120$ mm^3 centered 200 mm below the sensor array, the tracking system achieves the desired clinical goal.

Acknowledgments

First of all I would like to express my sincerest thanks to Dr. Parag J. Parikh for his guidance and support for the last two years. Without his help I would not be able to accomplish so much in my master's study. I would also like to acknowledge Dr. Joseph A. O'Sullivan for his help and directions.

I would like to thank Ryan Smith and Camille Noel for their generous help which enabled me to carry out clinical experiments. I also want to thank Jeff Newell and Jay Peterson for their help in providing technical details of the electromagnetic tracking system.

The research Calypso 4D Localization system was provided by Calypso® Medical Technologies (Seattle, WA). Stipend support was provided by the Washington University 4D Phantom program by Dr. Parikh. Research supported in part by R01CA134541.

Jie Wen

Washington University in St. Louis
May 2010

Dedicated to my parents.

I would like to give my deepest thanks to my parents who supported me through the whole graduate study and gave me the confidence and passion to make all the achievements. Without their support, I would not be able to be where I am today.

Contents

List of Tables

List of Figures

Chapter 1

Introduction

This thesis is focused on evaluating the performance of a wireless electromagnetic tracking system for tumor movement monitoring in a CT environment. Different error sources and their effects on the process of gathering position data are investigated. This chapter introduces the basic clinical expectations for this study and the potential use in Image Guided Radiation Therapy (IGRT).

1.1 Motivation

The goal of radiation therapy is to efficiently deliver the treatment dose to the specified cancerous tissues without harming the critical tissues such as the heart and other organs. The radiation to the surrounding tissue needs to be minimized in an effort to avoid serious side effects. In order to achieve this goal, sophisticated tumor positioning methods including motion tracking and deformation estimation are employed.

Respiratory motion has significant effects on abdominal and lung tumor position, and the uncertainty of the motion increases the treatment volume of the target due to a blurred tissue margin [1]. Respiratory correlated CT, which is obtained by oversampling images over the breathing cycles based on an external respiratory surrogate is applied widely in radiation therapy planning. The application of respiratory correlated CT is based on the assumption that the motion of the outside anatomy is reflective of the internal tumor or organ movement. This assumption is not always true in cases like weight loss, breathing pattern changes or non-respiratory motion, so, a tracking method that can directly provide the tumor position on a real-time basis is beneficial.[2][3]

Implantable passive transponders (Calypso® Medical Technologies) have been developed which can be tracked via an external sensor array in real-time and without ionizing radiation. Our goal is to integrate this wireless EM tracking device with a multislice CT scanner and provide volumetric datasets that are correlated to the internal tumor movement. The process of EM tracking while acquiring CT images is called as 'tumor correlated CT (TCCT)', which highlights the difference in using the internal tumor as motion as opposed to external anatomy as a surrogate for respiratory correlated imaging.

1.2 Goals for This Study

The fundamental goal for this study is to find out the proper working condition inside the CT environment in which electromagnetic tracking can be acquired concurrent with traditional CT image acquisition. A clinical goal of a maximum 2 mm error RMS on stationary tracking was set up as desired accuracy in tracking applications. The study also attempts to characterize the main sources of EM interference inside the CT environment and their effects on electromagnetic tracking.

1.3 Organization

There are three parts in this thesis. The first part introduces the background of the study and existing tracking technologies based on various methods. The clinical goals of this study will also be introduced. The second part focuses on introducing the experiment design in different research stages from primary tests for empirical data collection to comprehensive tests for determining the proper working volume and working conditions of the tracking system in a CT environment. The final part includes analysis giving the detailed performance evaluation of the tracking system and discussion of the outside factors that affect the accuracy and stability of the tracking system.

Chapter 2

Background

The first section of this chapter provides a brief introduction of clinical tracking technologies. The second section describes the medical environment: Phillips Brilliance Big Bore CT suite and sources of electromagnetic interferences present within this environment. The chapter concludes with a review of the theoretical framework of electromagnetic field theory pertaining to tracking systems and the nature of electromagnetic interference.

2.1 Overview of Tracking Technologies

In the past 30 years, a variety of tracking technologies, such as optical tracking, and electromagnetic tracking have been developed for motion capture/tracking in a wide range of fields including entertainment, sports and medical applications [4]. A tracking system is generally characterized by sample rates for data acquisition, precision, working range and degree-of-freedom (DOF). Each tracking system has its own advantages and disadvantages compared to other techniques according to the nature of the system and the applied areas.

2.1.1 Optical Tracking Systems

Optical tracking systems (OTS) consist of a receiver unit including two or more cameras and a set of special markers attached to the object. The 3D position of the markers can be calculated by using geometry and image processing on the images acquired from the stereoscopic cameras. Due to their fast sample rate, high accuracy, relatively isotropic measurement errors, OTS have found applications widely in clinical tracking use.

There are two types of optical systems based on the nature of the marker: Passive and Active. Passive optical systems use markers coated with a reflective material to reflect light back that is generated by light source near the cameras' lens. Rather than reflecting light back, active optical systems use powered markers. The markers actively emit light, e.g., illuminating LED. Based on the image acquired by each camera module, the position of the markers can be determined by data processing.

Optical trackers have high update rates and short lags. However, they suffer from the line-of-sight problem, e.g., any obstacle, ambient light or infrared radiation between the sensor and source will degrade the performance of the tracker. Therefore, the environment of OTS must be carefully designed to eliminate the uncertainty during the measurement. Additionally, this 'line of sight' requirement prevents optical tracking systems from use inside the human body.

One of the OTS applications in clinical use is called the Varian Real-time Position Management (RPM). The system contains an infrared source/camera pair fixed at a static position, and a target tracker box with marker dots made of reflective material on its surface placed on the patient's chest or upper belly for capturing the breathing cycle. Widely used in radiation therapy, the position information can be used for gating the treatment beam (Figure 2.1) [53].

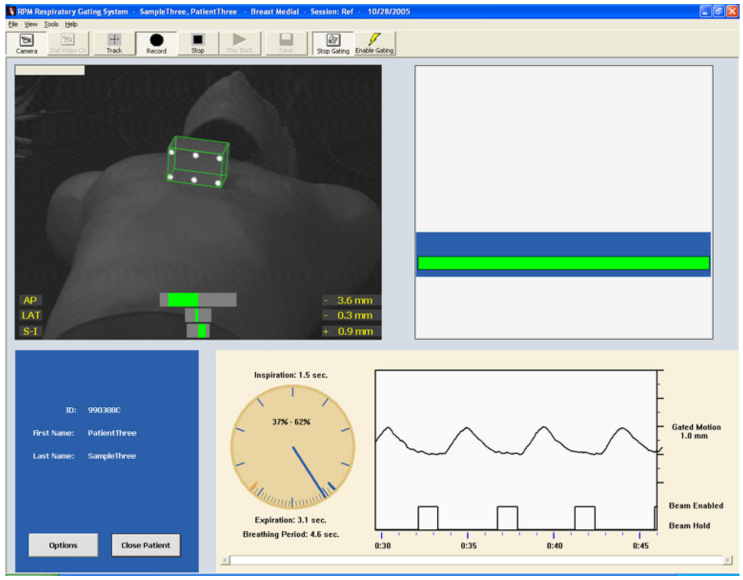

Figure 2.1 RPM Tracking Device and User Interface

2.1.2 Ultrasound

Ultrasound trackers usually use ultrasonic waves with frequencies above the audible range of human ear which is approximately 20 kHz. One basic form of ultrasonic tracker is a transmitter/receiver pair through which the distance information is obtained from the simple beat timing. This form is only for 1D distance checking. In order to realize a 3D localizing system, at least one ultrasonic source and three receivers are required as a minimum system configuration. For a better temporal resolution, three sets of transmitter/receiver pairs tuned at different frequencies need to be employed for simultaneous measuring.

Acoustic trackers utilize one of the following two techniques to determine position and orientation information: Time of Flight (TOF) and phase coherence. The TOF method uses a process of triangulation based on the known wave speed inside the media, time count on the wave transmission and the spatial distribution of the receivers. Phase coherence senses the phase difference between the single sent by the transmitter and that detected by the receiver. If the object being tracked moves more than half of the signal wavelength in any direction within the period of one update, there will be errors in the position determination. Since phase coherent tracking is an incremental form of position determination, small error in each update will result in accumulated errors over time.

For acoustic tracking systems, the limitations include the low speed of sound (340 m/sec in air and faster in denser media) which affects the temporal resolution of the tracking result, and the unstable speed caused by environmental variables like media density, surrounding temperature and air humidity. The requirement of media consistency and the reflection of the signal wave from hard surfaces also make the application of the system limited.

Given the nature of the limited working volume and accuracy, ultrasound tracking systems are commonly found in tracking applications where low precision object localization is required [5]. With improvements of the tracking algorithm and within a short tracking range, ultrasound devices are used to realize non-electromagnetic tracking achieving sub-millimeter accuracy and have been found useful in cardiology studies where minimum electrical signal is expected [6].

2.1.3 Mechanical Position Pointers

Mechanical digitizers are mostly used for motion capture and Virtual Reality applications. Some new 3D positioning pointers can also be used for 3D model building via 3D boundary capture. Their use was subsequently ported to medical tracking application before the use of optical tracking systems. Most mechanical digitizers used within medical environments consist of a passive arm with encoded joints.

Rotations and surface distances are measured by mechanical encoding devices like gears, potentiometers, optical encoders, etc. Based on a known starting point as the absolute zero point in the whole system, all the positions can be derived from relative movements of the whole encoded frame. One of the biggest advantages of the system is its real-time feature in the tracking process. The characteristic of the mechanical position encoder determines its low latency and high resolution which is useful in monitoring motion details. The position of the target can be solved by simply calculate over all the encoder values which also benefits the tracking speed of such system. Some new image guided surgery systems incorporating mechanical digitizers such as MicroScribe (Figure 2.2) [54] also provide haptic feedback which is a crucial element in real-time remote control surgery. The main limitation of such system is their relatively large size since the system needs to include feedback devices for all 6-DOF and short tracking range due to the necessity of proximity between the tracked target and the tracking device.

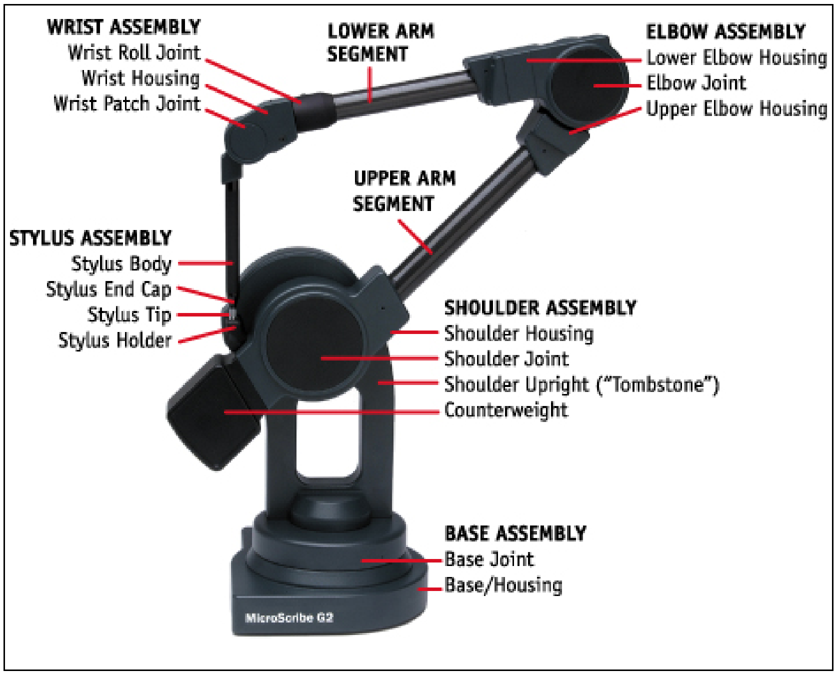

Figure 2.2 Diagram of MicroScribe Mechanical Tracking Station

2.1.4 Electromagnetic Tracking Systems

Electromagnetic Tracking Systems (EMTS) have found increasing use in medical applications during the last few years. Generally, EMTS consists of three components: field generator (FG), sensor unit and central control unit. The FG uses several coils to generate a position varying magnetic field that is used to establish the coordinate space. The sensor unit attached to the object contains small coils in which current is induced via the magnetic field. By measuring the behavior of each coil, the position and orientation of the object can be determined. Using this method, the positions of sensors are detected when moving within the coordinate space. The central control unit serves to control the field generator and capture data from the sensor unit. EMTS can provide three positions (X, Y, Z) and two or three orientation angles, and therefore are referred as 5-DOF or 6-DOF.

One important advantage of EMTS is that electromagnetic fields do not depend on line-of-sight for operation. Therefore, it has been used extensively in motion capture and virtual reality applications where complicated surroundings will limit the use of optical trackers by the line-of-sight requirement. Since EMTS depends on the measurement of magnetic fields produced by the FG or the transponder itself, the tracking units may be disturbed by the presence of any electronic device that produces EM interference. Another limitation of EMTS application is the trade off between system accuracy and working volume.

Different from an ideal point model, the strength of the electromagnetic field ν drops as a cubic function of distance r from a coil transmitter (2.1.a) [7][8]. In order to solve the position of a target, the algorithm is based on inverting (2.1.a) into (2.1.b) to find out the distance between the transponder and the receiver.

$$\nu \propto r^{-3} \quad (2.1.a)$$

$$r \propto \nu^{-\frac{1}{3}} \quad (2.1.b)$$

When given a distance calculation error Δr which is caused by a measuring error $\Delta \nu$, the relationship between Δr and $\Delta \nu$ is related to the derivative of (2.1.b):

$$\Delta r \propto \frac{dr}{dv} \Delta v \quad (2.1.c)$$

So, in this case when a interfering electromagnetic filed is constantly affects the volume of detection, the calculated position error (Δr) is expected to be proportional to the fourth power of the distance between the transmitter and the receiver ($d_{t\leftrightarrow r}$) (2.1.d).

$$\Delta r \propto d^{4}_{t\leftrightarrow r} \quad (2.1.d)$$

This error can be partially compensated by characterizing and estimating the interfering fields. With this said, system accuracy always degrades when the distance between the source and detector is increased.

There are currently several different commercial EM tracking systems for medical applications: Ascension microBIRD, NDI Aurora, Polhemus Fastrak and Calypso (Figure 2.3) [55][56][57][58]. The first three are wired tracking systems while the Calypso tracking system is the only tracking device which utilizes wireless tracking.

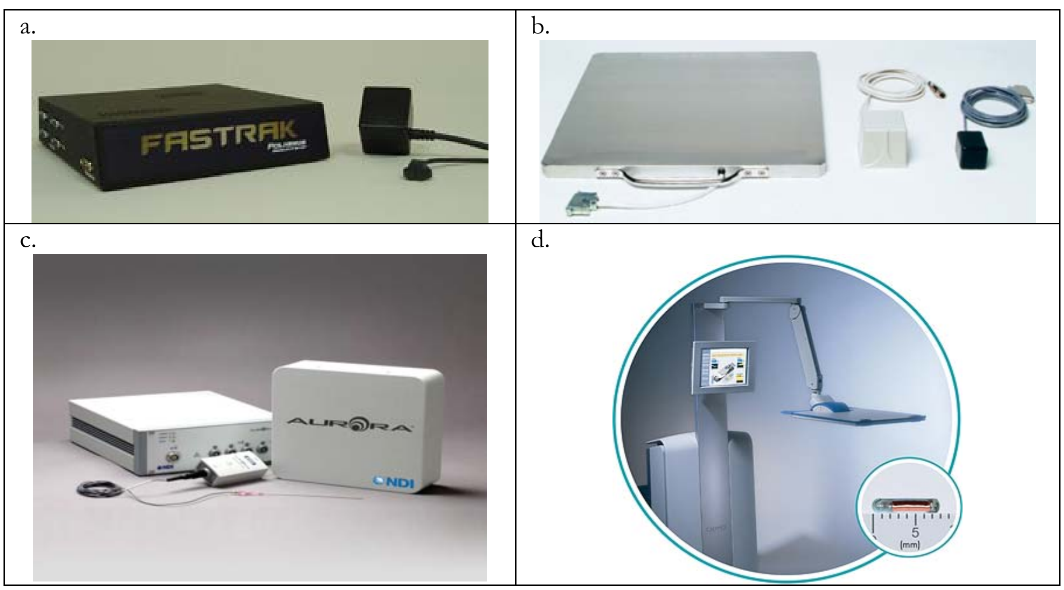

Figure 2.3 Electromagnetic Tracking Systems for Medical Applications: a. Polhemus Fastrak b. Ascension microBIRD c. NDI Aurora d. Calypso

In a wired tracking system there are two key components as shown in Figure 2.4: a field generator which will create electromagnetic field as the coordinates system; a set of wired sensor coils working within the reference field. At each point inside the reference field, the sensor coils can transfer back the field strength and orientation information through the signal wire. This information is used to determine the position and posture of the sensor coils inside this field (Figure 2.3 a-c). The Polhemus Fastrak and NDI Aurora systems use AC fields while the Ascention microBIRD system is based on pulsed DC field. The AC field tracking technology is believed to be superior to the DC systems since it is insensitive to the earth magnetic field either to the metal near the tracking system. The existence of unexpected metal inside the field will only introduce a static disturbance into the tracking volume which does not affect the distribution of the AC magnetic field, and therefore can be easily distinguished. Given the fact that the medical environment is usually complicated and lots of unexpected disturbances exist, this feature is valuable.

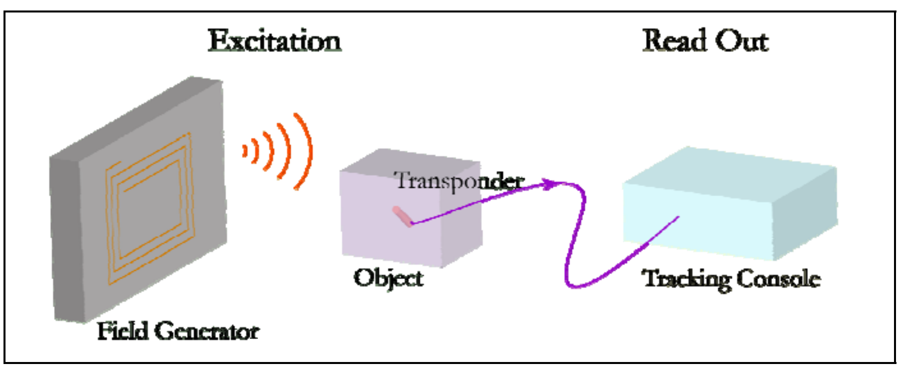

Figure 2.4 Schematic of Wired Tracking System

The NDI Aurora system has made the transition from virtual reality to medical applications through shrinking down the size of the sensor coils to make them small enough for skin insertion or bronchial therapy thereby achieving *in vivo* tracking. Furthermore, the Calypso tracking system enabled wireless tracking with signal coils small enough to be implanted with minimally invasive non-surgical procedures. The wireless feature largely benefits the patients and enables them move freely with the transponders implanted, which remain implanted indefinitely so no operation is needed to remove the transponders. To reuse the implanted wireless beacons, only simple position verification is needed each time before the tracking application and this is a huge advantage over wired tracking devices.

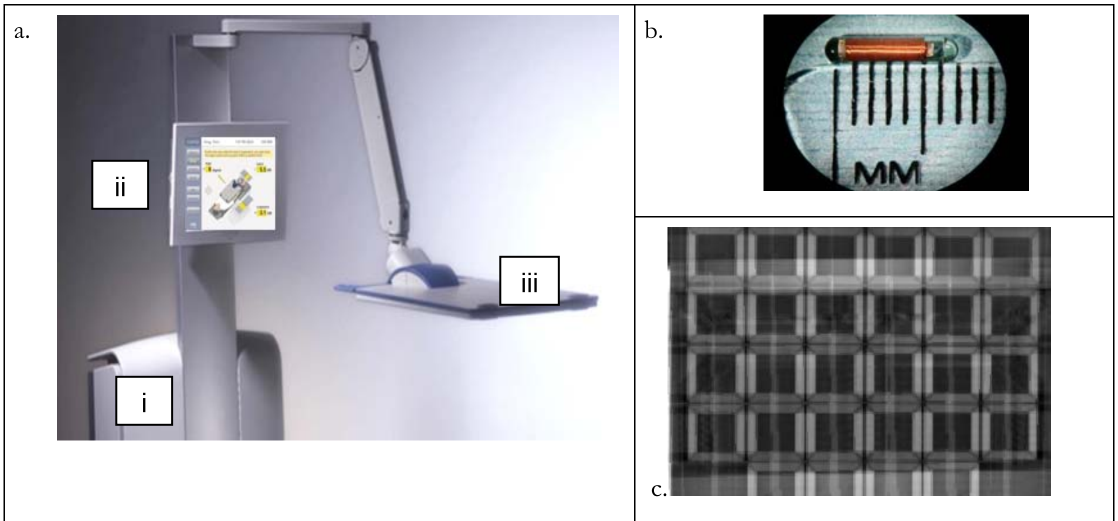

Calypso 4D Localization System. a. Calypso system console showing: (i) Console (ii) Real-time read out (iii) Tracking array/Field Generator. b. Beacon® transponder contains single coil shown with a ruler for scale c. X-ray image of sensor array (tracking antennas)[45]

Figure 2.5 Calypso Electromagnetic Tracking System Components

For wireless tracking devices, the system architecture is similar to wired products but with a different working procedure. In a wireless tracking system like Calypso, the transponder cannot directly send out the signal collected from the reference field, and as a result the tracking process is divided into two steps. The transponders used in the wireless system are tuned at certain resonance frequencies. First the tracking system emits a large power excitation signal at the resonance frequency and the transponder inside this field with the same characteristic frequency starts self oscillation. Then the excitation coils are turned off and an array of sensor coils (similar to an antenna array) will listen to the ring back signal sent by the working transponder. By evaluating the signal strength on each sensor coil inside the array, the position of the transponder can be determined using the tracking algorithm. Up to three transponders tuned at different resonance frequencies can be employed (Figure 2.6).

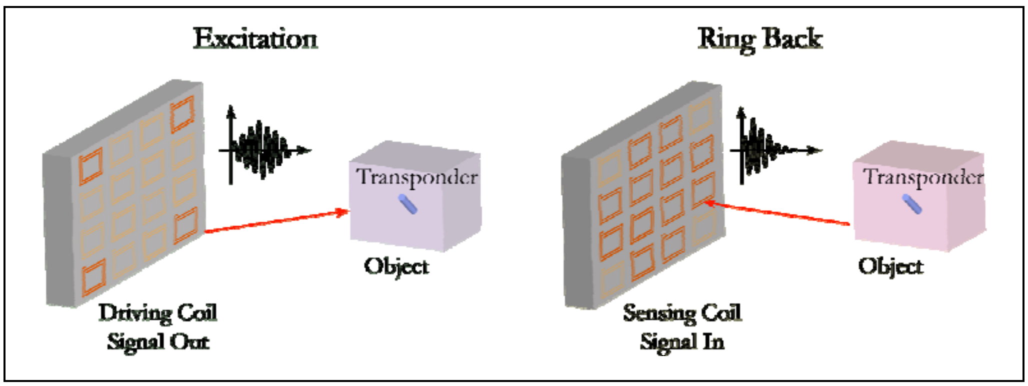

Figure 2.6 Schematic of Wireless Tracking System

The current Calypso tracking system has been integrated in the LINear ACcelerator (LINAC) environment (Figure 2.7, 8) [53][58]. The system includes a tracking console, a sensor array marked with infrared reflectors that are registered to the room coordinate system via stereoscopic cameras, and tracking beacons, which report position in 3 dimensions. The positions are available in real-time via a screen outside of the treatment area.

Figure 2. 7 LINAC System by Varian

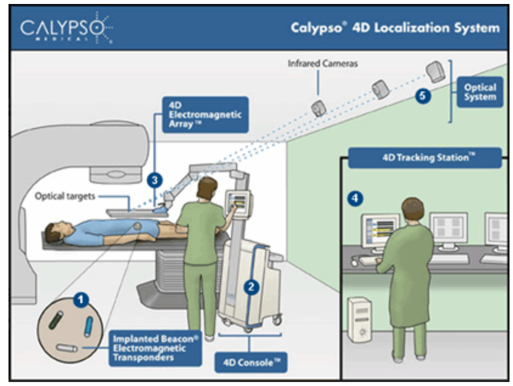

Figure 2. 8 Calypso Tracking System

Work has been published using the real-time position of electromagnetic transponders to modify treatment in the presence of motion [11]. In this system, dose is delivered only when the tumor is positioned optimally within the beam. Otherwise, when tumor moves outside the optimized margin, the beam will be turned off. This method ensures that the highest percentage of treatment radiation is irradiating the cancerous tissue and avoids the damage of surrounding normal tissue.

While there are still a lot of tracking technologies that could be added up to this list, it does provide a brief overview of the major tracking technologies used within clinical applications and their mode of operation. Other technologies such as inertial trackers and laser digitizers are used for tracking, however have found minimal use in medical applications. Fiducial tracking is another tracking method that uses fluoroscopy images to track gold seeds, which are implanted near tumor tissue and can be easily recognized in images. The Hokkaido system is a commonly used marker tracking system [9], but the requirement of constant irradiating patients limits its clinical use. Real-time imaging modalities like CT, PET or MRI are not mentioned here. Even though they are not strictly tracking technologies, their high spatial resolution enables image based position sensing with a low temporal resolution which is limited by the nature of the image acquiring procedure. Additionally, computation time associated with image processing limits their widespread clinical use.

2.2 Clinical Environments

The medical environment of interest in this study is Phillips Brilliant Big Bore CT Suite (Figure 2.9)[59]. Computed Tomography is a medical imaging modality whereby a 3D image volume is reconstructed from a set of 2D X-ray images through the use of the following reconstruction algorithms: Filtered Back-Projection, Integral Equations, Fourier Transforms and Series Expansion. The CT system, initially called Computed Axial Tomography (CAT), was invented in 1972 by Godfrey N. Hounsfield at EMI Central Research Laboratories. Since their inception, CT scanners have undergone four generations, with each subsequent refinement providing a reduction in data collection time and an increase in image quality [10].

Figure 2.9 Philips Brilliance 16 Slice Big Bore CT Scanner

Diagnostic CT imaging is done quickly while a patient holds their breath. This minimizes image artifacts due to respiratory motion. For radiation therapy, most patients would not be able to hold their breath during the whole radiation treatment. The radiation therapy planning CT (called the 'simulation CT') requires the imaging to match the treatment, so performing a simulation CT in a breath hold position may induce systematic errors if therapy is not being delivered with a breath hold. If the simulation CT is done during free breathing, there are artifacts due to respiratory motion and it is not clear that the respiratory artifacts will match all of the positions of the tumor during the breathing cycle.

In an effort to image tissue as it moves an imaging technology called 4D CT or gated CT has been developed to combine the traditional 3D CT with the patient breathing cycle. In this technique, conventional 3D CT is combined with an external respiratory surrogate such as a bellows affixed to the abdomen or a spirometer to record the breathing respiratory cycle throughout imaging. Images are oversampled at different phases and the final image set is grouped by different phase stamps as set up by a physician (Figure 2.10) [59]. At completion, a series of 3D CT images are generated in which the anatomy of each 3D image set is correlated with a specific phase/amplitude of the respiratory cycle, although different slices are typically recorded during different breaths. With this in mind, this imaging technique relies on both the reproducibility of breathing motion along with external/internal motion correlation.

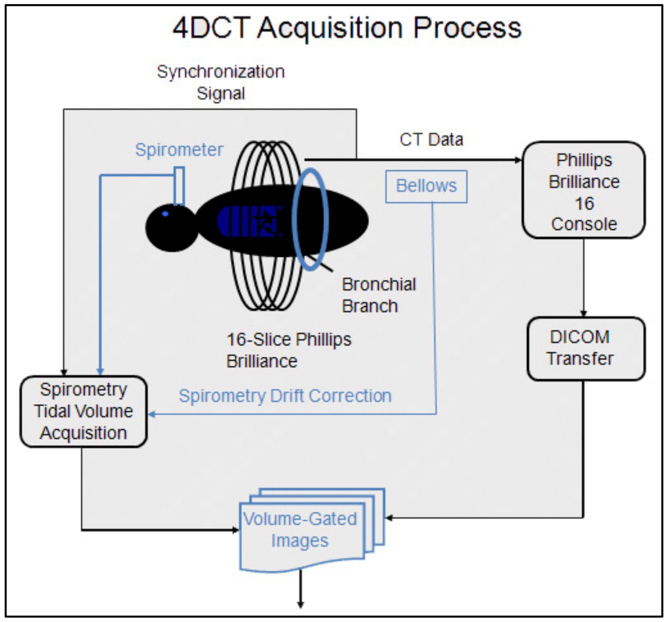

Figure 2.10 Overview of 4D CT System

In a LINAC environment, the main source of electromagnetic tracking noise is from the megavoltage ionizing beam. Since the high energy beam is working in a pulse form, the tracking system obtains the synchronized beam-on signal and stops tracking during the duty cycle. This method is effective at bypassing most of the noise introduced the LINAC. Also, there are moving metal parts in the head of the accelerator that can have some electromagnetic noise depending on the manufacturer, but this normally remains quite far from the patient. Similarly, the carbon fiber couch on the linear accelerator is replaced with a nonconductive material such as Kevlar so that it does not cause electromagnetic noise.

Comparing with the LINAC environment, the EM field inside the CT bore is more complicated since while acquiring images, there are moving metal parts in both the patient couch and X-ray tube/sensor. The nature of CT scanning requires a rotating pair of X-ray source and detector to measure the attenuation of X-ray passing through the imaging object. Besides the working pulse of X-ray which is crucial in the imaging process, the spinning of the large metal part will generate a changing noise field. Electromagnetic noise generated by the motor driving the arm also distorts the interaction between the sensor array and tracking beacons. Since the emitted X-rays are also a form of high frequency electromagnetic energy, this source will generate some baseline level of noise which is unavoidable. Further complicating the problem, these parts move in different manners depending on the scan type. Additionally the X-ray tube used in the CT scanner does not work in a pulsed mode like the LINAC X-ray source. The energy generated by the X-ray tube in CT applications is much lower (typically 120 keV) when compared with LINAC applications (6~15 MeV).

2.3 Electromagnetic Field Interference

Electromagnetic trackers first entered the market in the mid 1990s. They were used predominantly within computer graphics for animation, Virtual Reality (VR), and military applications. The advantageous of minimally invasive surgery techniques placed greater emphasis on imaging techniques for surgical navigation. This led to growing interest in electromagnetic tracking as an imaging modality. Several different approaches have been taken in the design of EMTS, however the principle of operation remains the generation of a coordinate system relative to the field generator.

The receiver is usually an array of coils that induces a current by changing the magnetic field inside the working volume. The basic theory governing this interaction between transmitter and receiver is Faraday's Law (2.2), which states that changes in the magnetic field will result in a potential difference (EMF, electromotive force) induced within the coil. The EMF then drives a current within the coils that can be measured. The magnitude of the voltage from the coil is proportional to the area circumscribed by the coil, the number of turns on the coil and the slew rate of the magnetic flux.

$$Emf = -N \frac{\Delta \Phi}{\Delta t} \quad (2.2)$$

N is the number of turns of the coil, $\Delta\Phi / \Delta t$ denotes the rate of change of magnetic flux. The negative sign is an indication of Lenz's Law which states that the induced force always attempts to oppose the rate of change.

A change in the magnetic field strength can be a result of different events, such as a variation of driving signal within the transmitter or a change of position or orientation between FG and receiver coils.

A frequency range was chosen to eliminate any line-of-sight restrictions. However, magnetic fields can be distorted by the presence of metal objects, especially when close to the tracking coils, which can lead to high errors. The main shortcoming of magnetic tracking systems is the limited detecting range. Despite this, electromagnetic tracking systems have seen widespread use because of their system topology, low price and most importantly lack of line-of-sight restrictions.

2.4 Error Compensation

Early work done to characterize EMTS was mostly conducted in the context of Virtual Reality (VR) applications. Only in the late 1990s, the studies of EMTS applications in medical environments started. The core of any of the EMTS application studies can be seen as either an attempt at quantifying the source of error or to set up an error compensation algorithm. Error compensation consists of three distinct approaches: 1) Analytical, 2) Local Interpolation and 3) Global Interpolation.

Experiments have been conducted using computerized fitting functions to define distortion sources within an electromagnetic measurement volume. These techniques assume that the distortion is a function of receiver position. A high-order polynomial can be used as an approximation of the error function. One of the earliest works to introduce this approach was by F. Raab and E. Blood [14]. The work shows that tracker error is proportional to the fourth power of transmitter-receiver separation and this kind of polynomial is proved to be a qualitatively sufficient method for defining the distortion. In more recent years, a concise and useful framework for calibration of errors in an EMT system is provided with studies conducted by three different groups: V. V. Kindratenko, M. A. Livingston and M. Ikits, *et al.* [15][4]. Of this, V.V. Kindratenko provides a comprehensive summary of various calibration techniques including tri-linear interpolation, shape functions, and high-order polynomial fits.

Various ways of error evaluation and compensation are widely applied in the VR environment. The application of the EMTS in the clinical environment still needs to be explored since even an unexpected working pulse from a DC-DC module inside any device can bring in large distortion to the detecting field and affect the tracking result. Therefore, it is believed to be important to evaluate the accuracy when the system is working in the clinical CT environment equipped with all devices where various distortions exist. By characterizing the effects of the possible noise sources, errors induced via EM field fluctuations can be mitigated/minimized.

Chapter 3

Experimental Design and Results

In this chapter, a series of experiments for characterizing the performance of the Calypso tracking system in a Phillips CT scanner are introduced. Empirically the factors which will affect the accuracy of a tracking device will be the environment background noise, working distance and outside metal objects. The working parameters of the tracking system such as the frontend amplifier gain, sensor array position inside the CT bore and implantable beacon orientation can also influence the tracking results. Experiments are designed to characterize the different sources of EM interference, as well as determine an optimal system setup to maximize tracking accuracy.

Table 3.1 Tested Items in Different Studies.

	Preliminary Test	Distance-Accuracy Study	Various Conditions Study	EM Field Characterizing
Target Distance	√	√		
Couch Metal Like Effect	√	√		
Gantry Spinning		√	√	√
X-ray Working Pulse	√	√	√	√
Array Position			√	
Array Gain			√	
Target Orientation			√	
Target Position			√	
Noise Distribution				√

3.1 Primary Test in CT Environment

3.1.1 Purpose

In order to use the Calypso system as an internal position monitor for TCCT acquisition, we must first determine the level of accuracy in the CT environment. The main purpose for this initial characterization experiment was to qualitatively evaluate the effects of distance between the sensor array and the tracking beacons. We believe the accuracy will go down when tracking beacons are moved away from the sensor array. This can be explained as follows. With the measuring distance increasing, the signal to noise ratio goes down as a result of the strength of the beacon signal decreasing while the background noise remains stable. In addition, the multipath effect inside the complicated detection area will cause the inaccuracy.

Another factor which we are interested in is how the existence of a carbon fiber patient couch, on which patient can be fixed and moved inside the CT bore during the scanning, will affect the tracking system. The carbon fiber is a polymer like component and possesses the advantages of light weight and high strength. Although suitable for conventional CT scanners, the metal-like behavior of a carbon fiber couch might cause undesirable interference for an EM tracking system.

3.1.2 Methods and Materials

The Calypso EM tracking system (Version 0.9.57) was moved into the Phillips Brilliant Big Bore CT suite. The sensor array was set up at the top inside of the CT bore and the beacons were positioned inside the CT bore under the center of the sensor array. Position measurements were taken in the absence of motion to determine the level of variation of the system.

The following modifiers were combined to form a total of 8 different runs: Beacons close/far from array, CT (X-ray tube) on/off, Couch in/out of the bore. The CT working parameters were chosen to simulate clinically relevant scans (Table 3.2):

Table 3.2 CT Running Parameters for Primary Test

Parameter Item	Parameter Value
X-Ray tube working voltage (kV)	120 kV
X-Ray tube working current (mA)	250 mA
Scanning cycle time	2 second
Gantry rotation speed	0.75 s/rev
X-ray tube working	On/Off
Gantry rotation	Static/Rotating

Array position was fixed at 25 cm above the patient couch. For the scans in which the beacons were placed close to the array, the exact position is 11.5 cm under the array (13.5 cm above the couch). For 'far' case, the beacons were positioned 21.6 cm under the array and 3.4 cm above the couch.

In a conventional CT scan there are parameters called the rotation time and the cycle time. The scanning (X-ray on) for each slice will last for a whole revolution of the sensor arm. This is defined as the rotation time. If the rotation time is less then the cycle time, the sensor arm will spin freely without emitting X-Ray until the scanning cycle time elapses. The next slice acquisition will begin at the completion of the cycle time, although the initial angle of the source/detector will likely be different than the initial slice.

3.1.3 Results

The standard deviations of position measurements for runs taken close to the array were considerably less than those of runs taken far from the array (Table 3.3). In addition, the existence of couch had a drastic impact on the position measurements when the beacons were sufficiently close to the couch (Figure 3.1). Standard deviations of over 1 cm were observed in various cases when beacons were far from the sensor array and couch was inside the bore. The observed results indicate that the hypothesized metal-like behavior of carbon fiber in the field of detection is a very large source of disturbance. The CT On variable provided higher standard deviations than Off in all cases, however if the beacons are sufficiently close to the array this effect should be negligible compared to other sources of error.

Table 3.3 Standard Deviations of Static Position Measurements (units in cm)

Distance	Couch Position	X-Ray Tube	stdx	stdy	stdz	MeanSTD
Close	In	On	0.03	0.04	0.02	0.03
Close	In	Off	0.02	0.01	0.02	0.01
Close	Out	On	0.11	0.09	0.09	0.09
Close	Out	Off	0.05	0.05	0.04	0.05
Far	In	On	1.51	1.56	1.38	1.48
Far	In	Off	1.10	0.88	0.83	0.94
Far	Out	On	0.41	0.41	0.40	0.41
Far	Out	Off	0.29	0.20	0.19	0.23

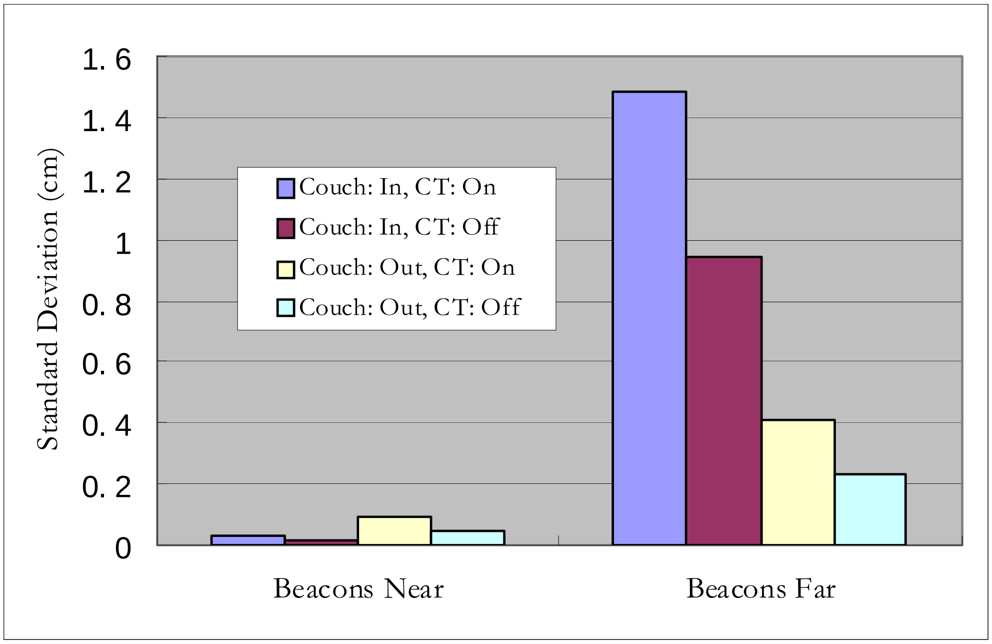

Figure 3.1 Standard Deviations for Various Modifiers

3.2 Study of Distance and System Accuracy

3.2.1 Purpose

Based on the results in the primary test in CT environment, one crucial factor that affects the level of accuracy of the tracking system is the position of the beacons, including the distance between the sensor array and the tracking beacons and the distance between the carbon fiber couch and the tracking beacons. At this point the detailed relation between the distance and the system accuracy needs to be studied. The results can be used to make an estimation of the working volume within the CT bore.

3.2.2 Methods and Materials

The research version Calypso tracking system (Version 0.9.57) was moved into the Phillips Brilliant Big Bore CT suite. The sensor array was inserted into the CT bore and positioned against the entrance of the bore. The laser beam inside the CT bore was turned on for aligning the tracking area with the isocenter of the bore, which is also the center of the imaging plane.

The patient couch was positioned inside the bore under the tracking area and 61.95 cm away from the bottom of the sensor array. Three beacons were fixed on a plastic slab vertically (Z orientation) and at the three vertexes of an equilateral triangle with side length of 3 cm. The plastic slab was placed on a stack of solid water sheets and by removing sheets the distance from the sensor array to the tracking beacons can be adjusted from 10.6 cm to 22.9 cm at a step of approximately 2 cm (Figure 3.2). Position measurements were taken when the beacons were placed steadily on the solid water stack and the standard deviation of the tracking data was used for evaluating the precision of the system. Tracking data for eight different positions ranging from 10.6 cm to 22.9 cm were recorded under both X-ray tube On and Off conditions.

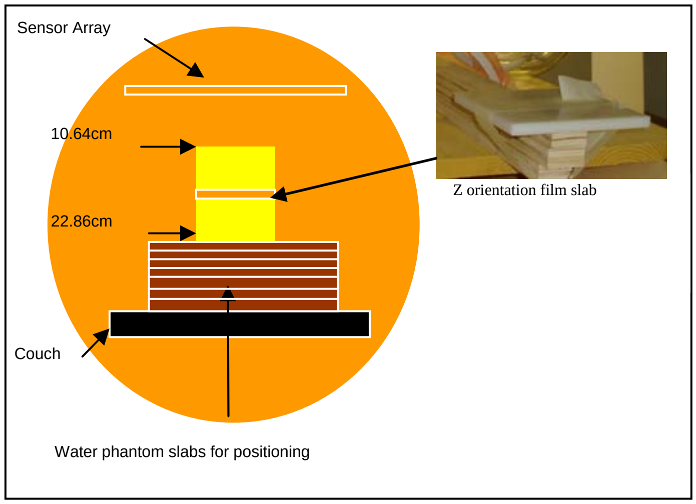

Figure 3.2 Experimental Setup

The CT parameters were chosen as ordinary clinical application:

Table 3.4 CT Running Parameters for Distance-Accuracy Study

Parameter Item	Parameter Value
X-Ray tube working voltage (kV)	120 kV
X-Ray tube working current (mA)	250 mA
Scanning cycle time	2 second
Gantry rotation speed	0.75 s/rev
X-ray tube working	On/Off
Gantry rotation	Static/Rotating

3.2.3 Results

Eight sets of tracking data were recorded and STDs were used to evaluate the precision of the system. The result shows a steady trend of increasing standard deviations when the tracking beacons are positioned further away from the sensor array (Table 3.5). The distance affects the level of accuracy in CT Off/On tests. From Figure 3.3 one conclusion is that the noise level rises as the distance increases. The X-ray tube working pulse also affects the accuracy level which is shown clearly in Figure 3.3 that the CT On curve exhibits higher standard deviations than the CT Off curve for all measurements. Furthermore, with the distance increases, the influence of X-ray source on the accuracy also increases. Fourth order polynomial fitting is applied to both CT Off and CT On data sets and yields good agreement with the fitting residual of 0.003 cm.

Table 3.5 Standard Deviation of Static Position Measurements

Distance (cm)	**CT OFF**			
	STDx	STDy	STDz	Mean STD
10.64	0.0105	0.0097	0.0057	0.0086
12.38	0.0715	0.0392	0.0472	0.0526
14.45	0.1034	0.0624	0.0688	0.0781
16.35	0.1430	0.1061	0.0833	0.1108
18.26	0.2132	0.1775	0.1152	0.1686
20.32	0.3673	0.3016	0.2406	0.3032
22.86	0.7014	0.6503	0.4293	0.5937
	CT ON			
10.64	0.0315	0.0337	0.0363	0.0338
12.38	0.0795	0.0682	0.0544	0.0674
14.45	0.1211	0.1054	0.0850	0.1038
16.35	0.1814	0.1541	0.1166	0.1507
18.26	0.2715	0.3298	0.1834	0.2616
20.32	0.4836	0.5656	0.4238	0.4910
22.86	0.9349	0.9611	0.7194	0.8718

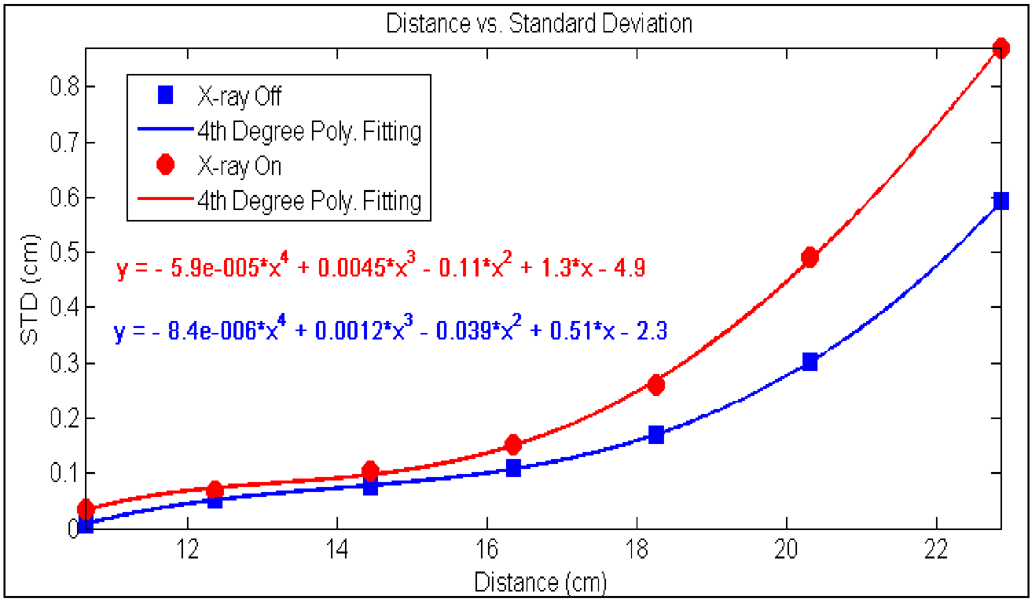

Figure 3.3 Standard Deviation for Different Positions: CT On/Off

The carbon fiber patient couch is fixed 61.6 cm away from the sensor array and the closest point from the beacons to the couch during the experiment is 38.7 cm where the largest distance between the sensor array and the tracking beacons (22.6 cm) is obtained. The standard deviation of the CT Off tracking measurement is 0.59 cm while 0.87 cm for CT On. Recalling the results from the primary test in the CT environment when beacons were placed 21.6 cm away from the sensor array and the distance between the couch and the tracking beacon was 3.4 cm, the standard deviation for CT Off and CT On tests were 0.94 cm and 1.48 cm, respectively. If neglecting the 1.2 cm difference of the distance from beacons to sensor array in the two tests, the only difference is the distance from the patient couch to the tracking beacons which was 3.6 cm in the first experiment and 38.74 cm in this test, but the resulted standard deviation of the tracking data got a 60% improvement in CT Off test and a 70% improvement in CT On test in this experiment. The results prove the assumption that the distance from the beacons to the carbon fiber couch can affect the tracking accuracy, while more importantly, when carbon fiber couch is far enough from the beacons, the tracking system can still work even without removing the couch.

The power spectrum of the tracking data shows a clear interference from the rotary metal part inside containing the X-ray tube and sensor along with their supporting components. The spinning speed of the metal arm was set to 0.75 s/revolution which is a motion with a characterized frequency of 1.33 Hz. The scanning period was set to 2 seconds which is a periodic signal with 0.5 Hz frequency. In power spectra of all the tests under CT On condition (Figure 3.4), these frequency elements with high power density could be identified easily which imply the spinning metal inside the gantry and the X-ray tube working pulse are the key sources of noise in CT environment.

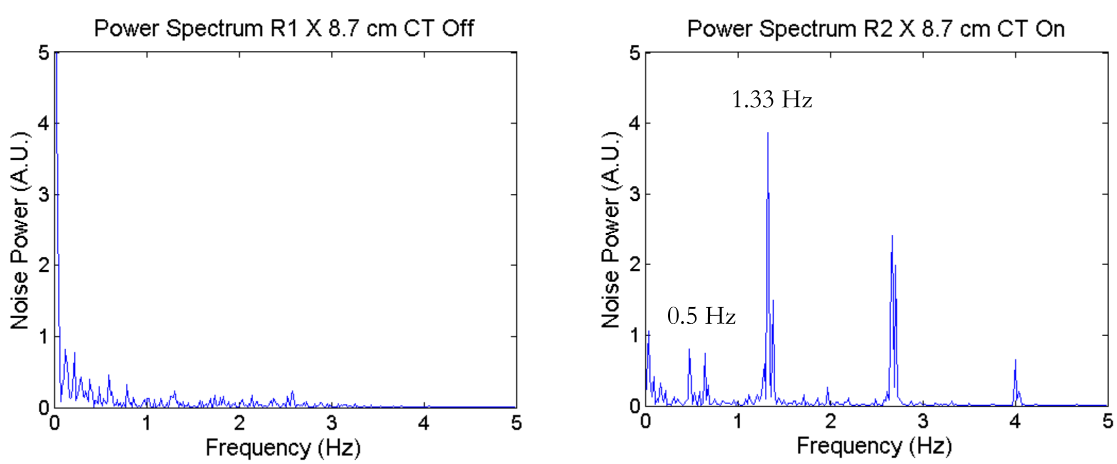

Figure 3.4 Power Spectra: CT Off vs. CT On

3.3 Various Working Condition Study

3.3.1 Purpose

In order to use the Calypso system in a CT environment, intensive study of the tracking system performance under different working conditions with various environmental parameters is necessary. Previous studies analyzed the precision dependence of the clearance between the carbon fiber patient couch and the beacon slab. Other working parameters including frontend amplifier gain, beacon position, sensor array position and beacon orientation all need to be considered.

Frontend amplifier gain is an adjustable variable that could be set to high or low in the research version user interface of the Calypso system. This variable controls the front end amplifier which could be set to low when working in a complicated electromagnetic environment and high when working in environment with relatively lower level of electromagnetic disturbance.

The sensor array provides a working area of 14×14 cm^2 and can track positions up to 27 cm away from the array plane within this area. For all the previous tests, the tracking beacons were placed under the geometric center of the sensor array which is the optimal working position. In actual clinical application, the beacons' implanted position varies for each case, thus, centering the beacons in tracking process could be optimized but can not be guaranteed to get a perfect alignment in all cases. Therefore, the tracking performance of the system with beacons on the boundary of the working volume needed to be studied to verify if the system can achieve the desired accuracy throughout the whole tracking volume.

Beacon orientation is another factor which affects the tracking accuracy. The working procedure of the Calypso tracking device is divided into 3 steps:

1. The four large source coils inside the array send out an excitation signal at the beacon's resonance frequency.

2. When the excitation signal is turned off, the transponder signal during relaxation is measured by 32 sensor coils inside the array.

3. An algorithm is applied to get the 3D Beacon position based on the magnitude of the signal from each detector coil. Oversampling and filtering algorithms are used to optimize the reliability of the tracking result.

4. Steps 1-3 are repeated several times for each measurement until the variance is acceptable indicating an accurate position measurement has been made.

The tracking plate is placed in a fixed position. The source coils in the tracking plate will provide a steady excitation field and the sensor coils in it will evaluate the Z direction components from the tracking beacons in oscillation. When beacons are put into the field at different angles, the excitation efficiency will be different and the ring back signal will be coupled into the sensor array with various signal strengths. The uncertainty of the signal coupling from excitation to ring back could affect the system accuracy and as a result this should be characterized.

3.3.2 Methods and Materials

The research version of Calypso tracking station was moved into Philips Brilliant Big Bore CT suite. The CT table top was replaced with a custom made wooden couch in order to eliminate the metal like effect from the carbon fiber material.

For analyzing how beacon orientation affects accuracy, two sets of beacons were employed in the experiment aligned in orthogonal directions along the Z and Y axis (Figure 3.5). For the Z orientation, a plastic slab used in previous studies was employed and the beacons were vertically placed with the coil axis pointing at the sensor array. For the Y orientation, the beacons were placed horizontally with primary axis parallel to the sensor array and aligned with the axis of the CT bore. The two orientations are actually two extreme cases of the possible beacon posture when it is implanted into an actual patient for tracking. The two postures can be used to evaluate the relationship between tracking accuracy and beacon orientation.

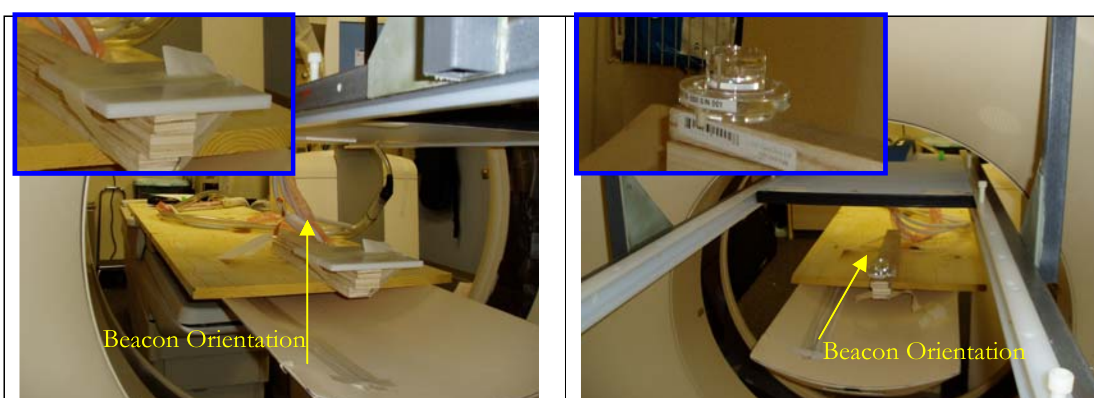

Z orientation beacons | Y orientation beacons

Figure 3.5 Tracking Beacons Inside CT Bore

The sensor array was placed inside the CT bore while tracking and aligned at two positions: Array Low and Array High. This pair is used as a reference group to compare the disturbances brought in by the metal elements inside the CT bore at different distances. The Array High is defined as the top of the sensor array positioned 14 cm away from the CT bore intrados, and correspondingly Array Low is defined as the top of the sensor array positioned 26 cm away from the CT bore intrados. The array board was taken off from the arm of the tracking station for more flexible positioning and was placed on an array holder which can hold the sensor array and the beacons together to provide an absolute position reference from the sensor array to the tracking beacons.

The tracking station has adjustable front end amplifiers which serve the sensor coils and can be switched between Gain Low and Gain High depending on the surrounding noise.

CT scanner working parameters are set as the table below (Table 3.6) which is a typical clinical set up.

Table 3.6 CT Running Parameters for Various Working Condition Study

Parameter Item	Parameter Value
X-Ray tube working voltage (kV)	120 kV
X-Ray tube working current (mA)	250 mA
Scanning cycle time	2 sec
Gantry rotation speed	0.44 s/rev
X-ray tube working	On/Off
Gantry rotation	Static/Rotating

In order to evaluate the influences brought in by the nature of CT scanning, the gantry arm was set to the following working status:

1. Static position Anterior Posterior (AP) mode with X-ray off.

2. Arm spinning at 0.44 sec/rev. with the X-ray tube on.

3. Arm spinning at 0.44 sec/rev with the X-ray tube off.

In order to estimate the experimental error, measurements were taken outside the bore with the X-ray arm static and CT off. These measurements were taken both before and after all the in bore measurements as a stand alone reference which can be used in estimating the error bar over the experiments.

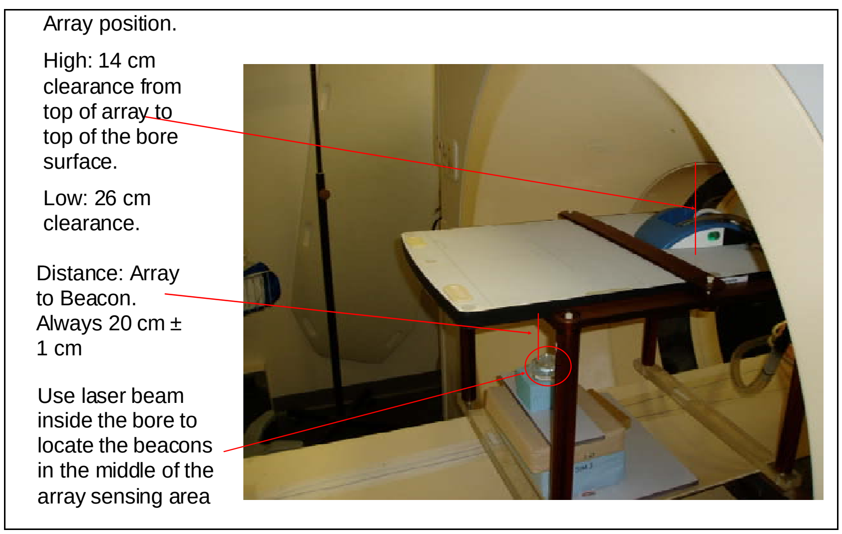

Figure 3.6 Experimental Setup

For each different working form, five measurements were included as a group. Three were tested inside the CT bore under different working conditions and two were tested outside the CT bore for reference (Table 3.7). The working flow of each group is as following:

a. Outside Bore Static: Before all the tests with inside bore parameters start, a set of tracking data is taken outside the bore without gantry arm spinning and X-ray tube working. This test can be used as an estimation of the background noise since in this test the whole tracking system is working outside the CT bore and the CT scanner is in the standby mode, introducing no interference to the tracking accuracy. The results can be interpreted as the base line performance of the tracking system, since without any CT scanner activity the result shows the system tracking accuracy in a general medical environment.

b. Inside Bore Static: Tracking system works inside the CT bore with no other motion or X-ray tube working.

c. Inside Bore Spinning: Tracking system stays inside the bore with the source/detector spinning and the X-ray tube off.

d. Inside Bore Spinning: Tracking system works inside the bore while the CT scanner is doing an ordinary slice scan with X-ray arm spinning and X-ray tube working under clinical set up as Table 3.5.

e. Outside Bore Static: Duplicate test (a) as a reference group. This reference test is also useful when estimating the experimental error.

Table 3.7 Test Cases

<table>
<tr><td rowspan="3">Test group design</td><td colspan="2" rowspan="2">Array Position High (14 cm to the top of the bore)</td><td colspan="4">Array Position Low (26 cm to the top of the bore)</td></tr>
<tr><td colspan="2">Beacon Centered</td><td colspan="2">Beacon Shifted to edge of testing area</td></tr>
<tr><td>Beacon orientation Z</td><td>Beacon orientation Y</td><td>Beacon orientation Z</td><td>Beacon orientation Y</td><td>Beacon orientation Z</td><td>Beacon orientation Y</td></tr>
<tr><td rowspan="5">Data collected for each group</td><td colspan="6">Outside bore static mode (First time)</td></tr>
<tr><td colspan="6">Static AP mode</td></tr>
<tr><td colspan="6">Spinning without X-ray</td></tr>
<tr><td colspan="6">Spinning with X-ray</td></tr>
<tr><td colspan="6">Outside bore static mode (Second time)</td></tr>
</table>

3.3.3 Results

The results of the tests with frontend amplifier gain set to high showed a very high error rate through the whole tracking process. The RMS error over the high gain tracking tests was 4.5 mm which is 125% over the expected accuracy for clinical use. The Tracking tests with sensor array set to low gain get results in achieving the clinic goal (RMS error <2 mm) independent of beacon orientation or CT acquisition (Figure 3.7). Results obtained when the sensor array position is low show significant improvements comparing with the results of the sensor array placed in high position. The maximum error rate appears when beacon orientation is Z and acquisition is performed at the periphery of the detection volume (7 cm lateral shift from the center).

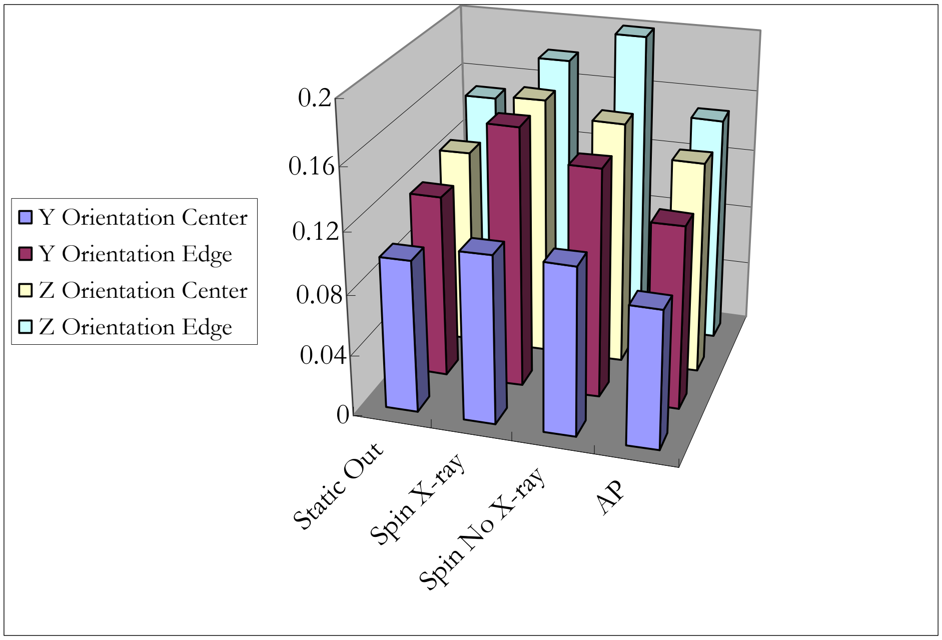

Figure 3.7 Performance Overview, Array Position Low, Gain Low

The arm spinning inside the gantry is the largest noise source. Beacons/ Array shifting off the bore center shows a slight effect on the tracking accuracy when tested with the beacons in Z orientation. The effect is even smaller when the beacons are in Y orientation.

3.3.4 Discussion

3.3.4.1 Spinning Metal

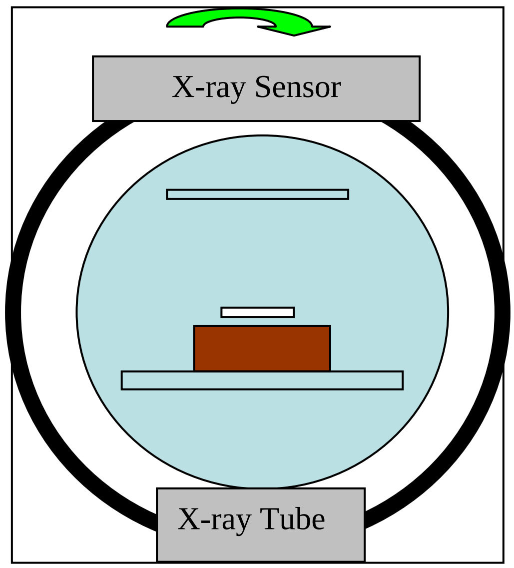

Figure 3.8 Spinning X-ray Arm Inside CT Bore

The X-ray arm is a large piece of metal spinning inside the CT bore (Figure 3.8) which will change the magnetic permeability, thus modulate the stimulating magnetic field. Furthermore, remanence of the rotating part is an additional alternating magnetic field, and can affect the measurement by disturbing the field distribution inside the measuring volume which is not considered in the algorithm.

3.3.4.2 X-ray Tube Working Noise

The X-ray tube working does not contribute much noise when compared with the main noise source generated by the spinning metal inside the gantry. The X-ray tube consists of two parts. One is the heating part in which a small AC power is applied to the filament for heating the material in order to release electrons. The other part is a very high DC voltage which is added between the filament and the anode for accelerating the electrons to a tungsten target in order to generate X-rays (Figure 3.9)[60].

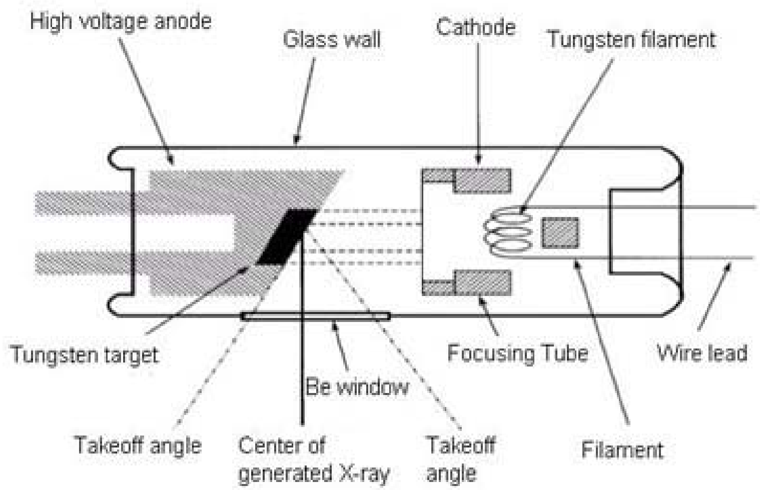

Figure 3.9 X-ray Tube Structure

Since the DC accelerating voltage does not generate any distortion to the tracking device, the only source of noise from the X-ray tube is the AC heating current which is relatively small. That is why when comparing the results of inside bore spinning CT On/Off power spectra, only limited difference of power distribution could be found by visual comparison.

3.3.4.3 Beacon Orientation

The orientation of the beacon can also affect the tracking accuracy. Figure 3.14 shows the simulation result of the magnetic field distribution for different orientations of a single beacon inside the excitation field generated by the sensor array using finite element method. If the array is aligned in the same direction with which the radiation energy is focused, and simultaneously, the polarization directions of the beacon and the array (as an antenna) are matched well, there will be strong coupling and the signal to noise ratio (SNR) will be high (Figure 3.10a). On other hand, if the array is not in the proper direction or the polarization directions of the beacon and the array are not matched, the coupling will be weaker (Figure 3.10b).

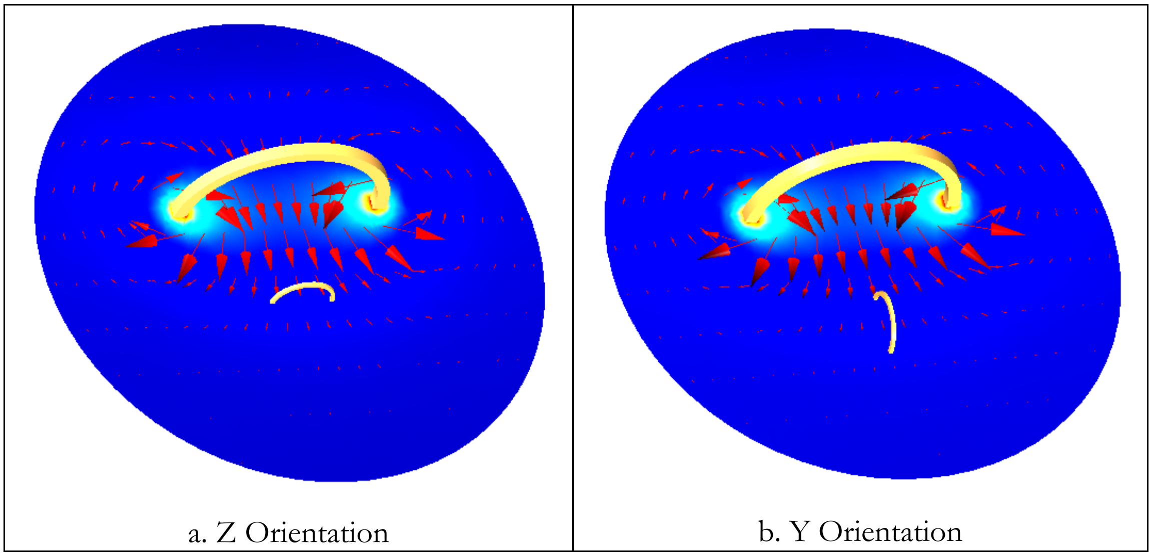

Figure 3. 10 Illustration for Coil Orientation in Excitation Stage. Arrows denote the magnetic field distribution.

Since the system uses an antenna array to measure the strength of the ring back signal, both the excitation and the reading stage will affect the tracking results. Coupling of the signal into the sensor array will be affected by not only the surrounding noise but also the orientation of beacons. The sensor array uses square shaped coils with the axis placed vertically to receive component of the magnetic field in Z direction which is the only component that the Calypso system is sensitive. So if the beacons are placed in Z orientation, it is a best fit to couple the signal, while in Y direction the coupling is weaker since only part of the ring back signal gets into the sensor coil. This kind of evaluation on strong or weak coupling lies on the absolute strength of the signal. However, in tracking application, the system relies on evaluating the differential signal over the whole sensor array and the system accuracy relies on the sensor array's sensitivity to the step change of magnetic flux caused by position movement. Figure 3.11 shows the simulation results of the magnetic field generated by the tracking beacon in the ring back stage by finite element method. The beacon is simplified as a one turn coil put under the sensor array in both Z (Figure 3.11 a) and Y (Figure 3.11 b) direction. The 6x6 sensor array is simplified into a 2x1 array for better visual result.

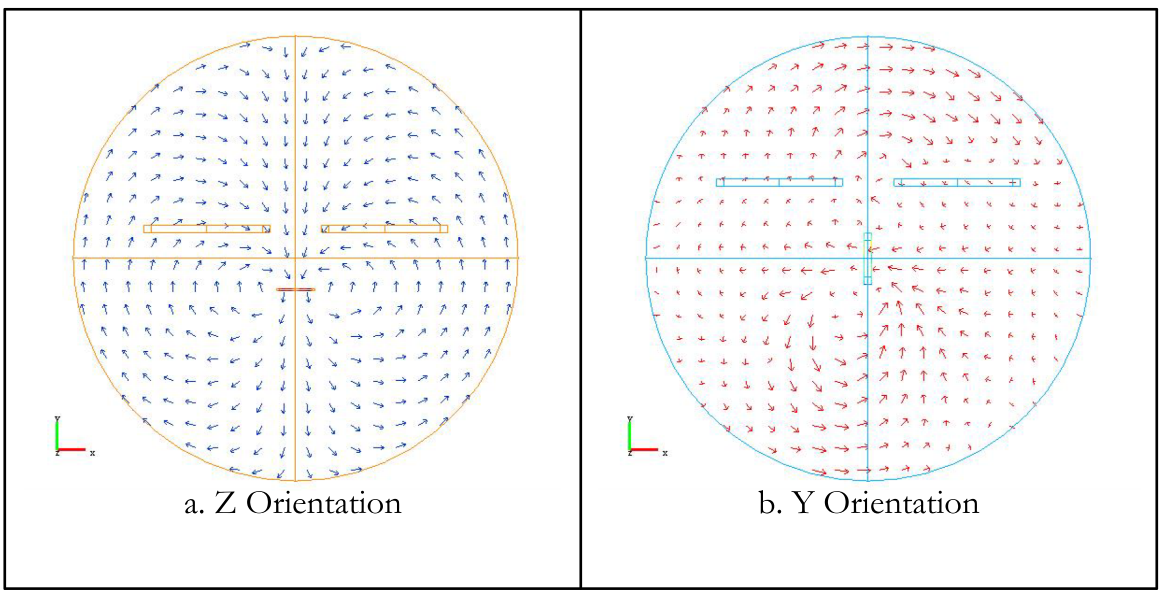

Figure 3.11 Illustration for Coil Orientation in Ring Back Stage. Arrows denote the magnetic field distribution.

When the tracking beacon is excited by a strong driving signal tuned at its resonance frequency, it will start self oscillation and establish a ring back electromagnetic field. The antenna array evaluates the magnetic flux change over the whole array to determine the object position. It is clearly showed in Figure 3.11 a-b that with a Z orientated beacon the Z component of magnetic flux on antenna is determined by $\phi=\phi_{in}-\phi_{out}$. When position changes, the change in measured magnetic flux is smaller when compared with the Y oriented beacon since the direction of the magnetic field passing through the antenna is uniformed and $\phi=\phi_{in}$. In other words, Y-oriented transponders result in greater change in measured magnetic flux per change in position than do Z-oriented transponders which implies the Calypso system is more sensitive to changes in position of a Y-oriented transponder than to changes in a Z-oriented transponder. In solving for a position estimate based on measurements of magnetic flux in the presence of external interference, it is therefore easier to perturb the solution of a Z-oriented transponder than it is for a Y-oriented transponder for the same amount of external interference. This explains why the tracking system has better tracking accuracy with tracking beacons in Y direction.

3.4 Electromagnetic Field Characterization

3.4.1 Purpose

Electromagnetic field fluctuation inside the tracking volume is a large source of disturbance to the tracking algorithm which leads to degradation in system accuracy. The complicated EM field inside the CT bore cannot be modeled simply by accumulating all the possible noise sources, so a characterization experiment was necessary to determine the optimal working conditions for the Calypso system in a CT environment.

3.4.2 Methods and Materials

A fiber glass frame for attaching test piece to the CT bore is combined with a fixture designed for holding a solenoid at various locations inside the CT bore (Figures 3.12-13). The carbon fiber couch was removed in order to eliminate the metal behavior disturbances.

Figure 3.12 Fixture Holding the Solenoid Inside CT Bore

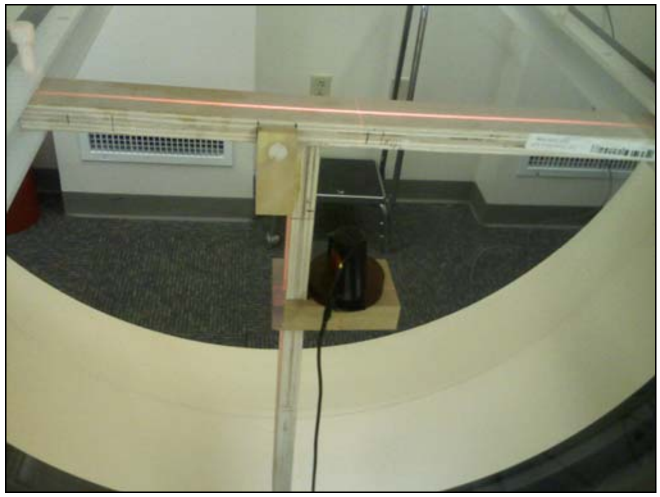

Figure 3.13 Detailed Alignment Inside CT Bore

The solenoid used in the measurements has the following characteristics: The coil length is 2.4 cm and the coil diameter is 2.54 cm. The solenoid has N=213 turns of coils (Figure 3. 14). Given the cross area of the coil as $A = \pi r^2$, the effective area of this solenoid is $N \times A = 213 \times \pi \times (1.27 \text{ cm})^2 = 0.108 \text{ m}^2$, and the inductance of the solenoid is 870 μH. The solenoid was oriented vertically in the testing volume. Only one orientation was deemed necessary due to the symmetry associated with the bore rotating around the isocenter (Figure 3.15).

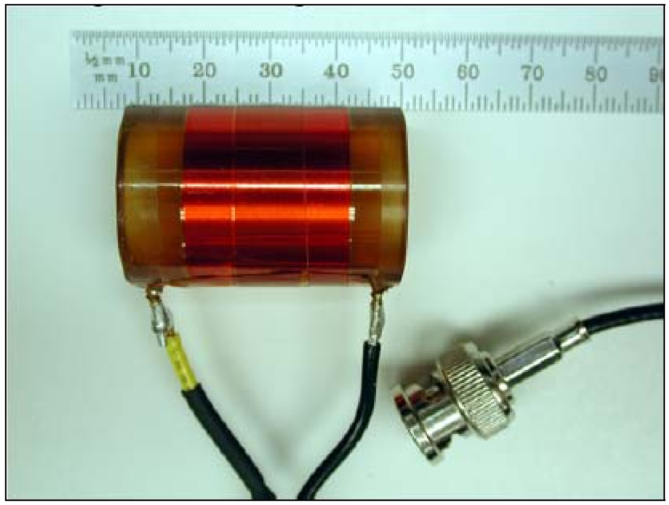

Figure 3.14 Solenoid Used in Experiment

Considering the working volume of the tracking system (14×14×14 cm) we determined to record the magnetic field over a large volume of 48×44×44 cm^3 centered around the isocenter of the CT bore covering the whole working volume. Data was taken as a 3×3×3 grid occupying the testing volume. Two additional runs were recorded outside the bore 49.5 cm away from the isocenter of the bore (Figure 3.15).

Data point index: Green plane is the axial plane contains the isocenter of the bore. Purple plane contains 9 data points 22 cm away from the front of the isocenter plane. Orange plane contains another 9 data points 22 cm away from the back of the isocenter plane. Front/Back Outside Bore points are 49.5 cm away from the isocenter on both sides.

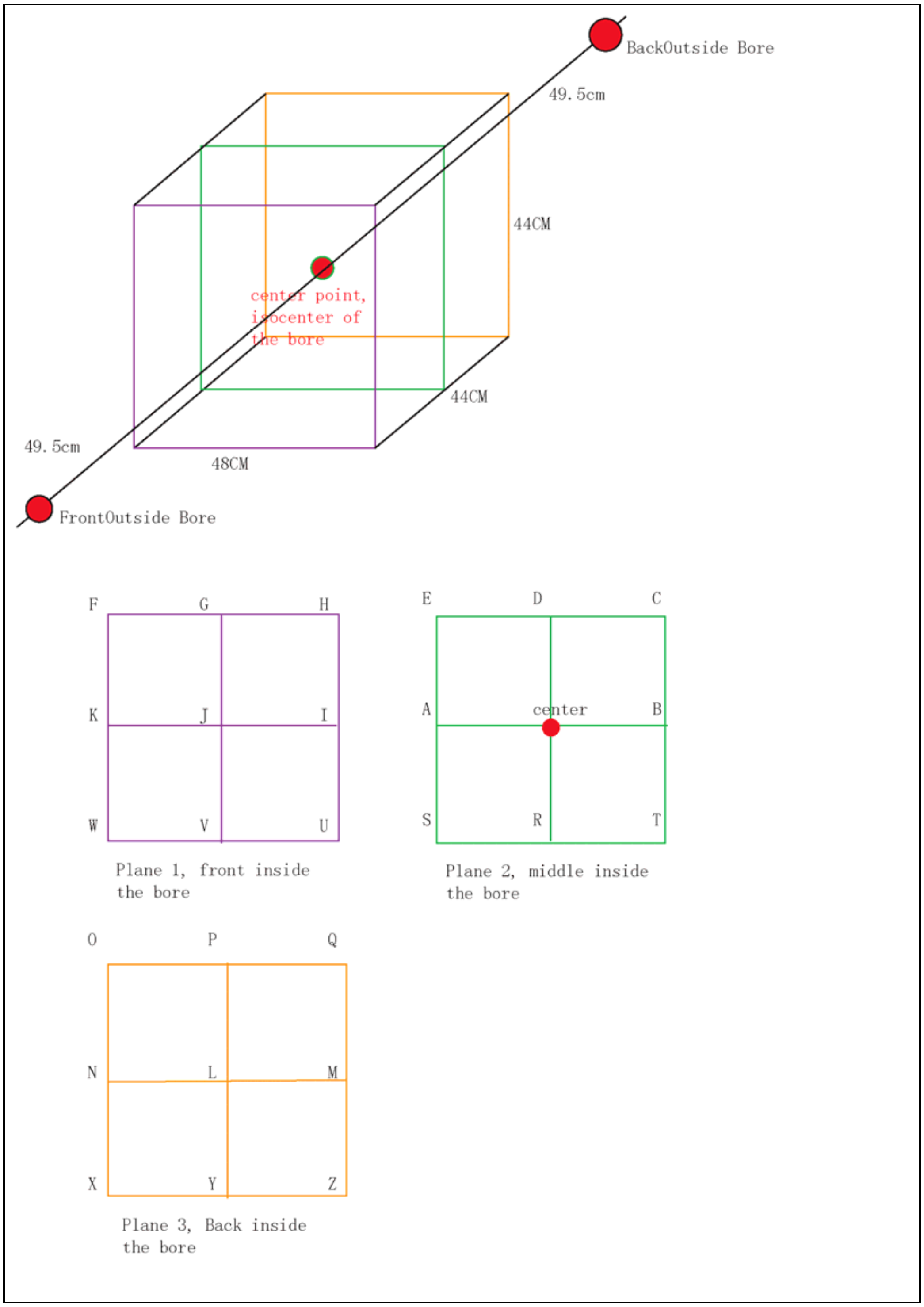

Figure 3.15 Testing Volume and Measuring Point Position

The CT scanner running parameters were set as Table 3.8:

Table 3.8 CT Running Parameters for EM Field Characterize

Parameter Item	Parameter Value
X-Ray tube working voltage (kV)	120 kV
X-Ray tube working current (mA)	250 mA
Scanning cycle time	1 sec
Gantry rotation speed	0.5 s/rev
X-ray tube working	On/Off
Gantry rotation	Static/Rotating

A Tektronix 3300B oscilloscope was connected to the solenoid to record the current which is analogous to the strength of the magnetic field at each position. The testing circuit is shown in Figure 3.16.

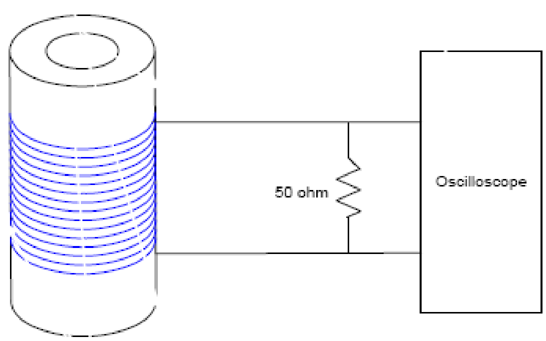

Figure 3.16 Schematic of Testing Circuit

3.4.3 Results

A 4 ms cycle can be observed for R point (Figure 3.15) from the measured waveform (Figure 3.17b) which indicates a low frequency modulation at this point. Figure 3.17a shows the normal pattern of the signal picked from the solenoid when X-ray is off.

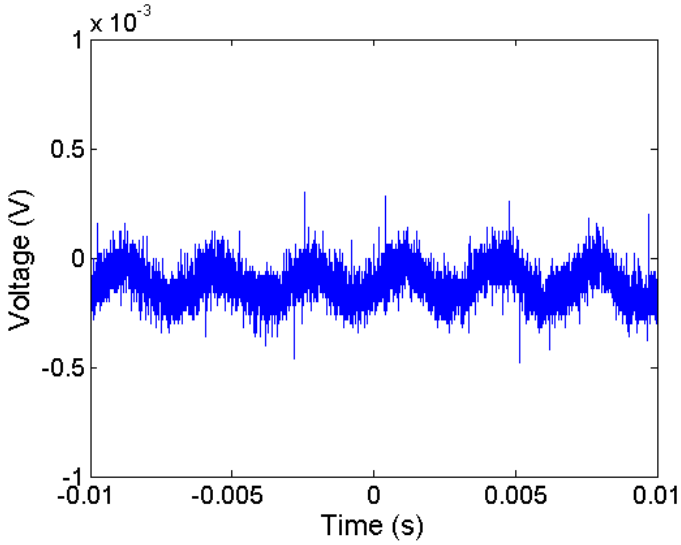

a. X-ray Off

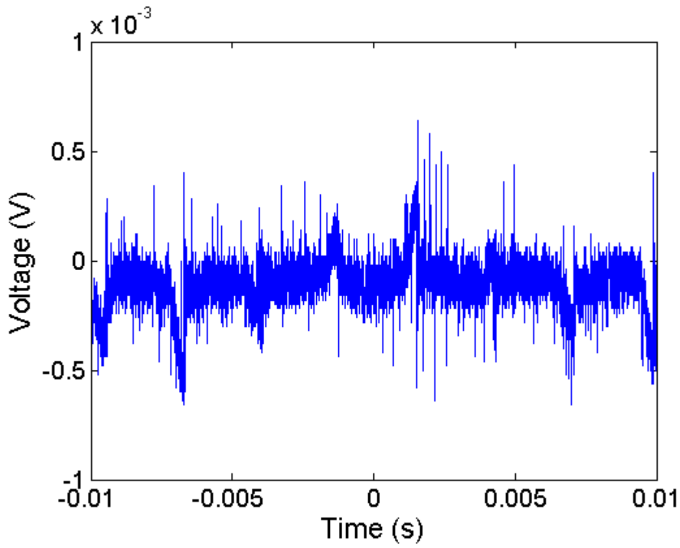

b. X-ray On

Figure 3.17 Typical Waveforms of the Solenoid

To study the frequency distribution of the noise on different bands, the noise power is integrated around the center frequencies of 1.25 kHz, 10 kHz and 20 kHz, respectively, for each data point and the results are shown in Figure 3.18. The noise power is larger on the center plane than the other two outer planes for all three bands. With the increment of frequency, the attenuation of the noise power from the center plane to the outer planes increases, indicating that the noise of high frequency is more concentrated on the center part of measurement volume than that of the low frequency.

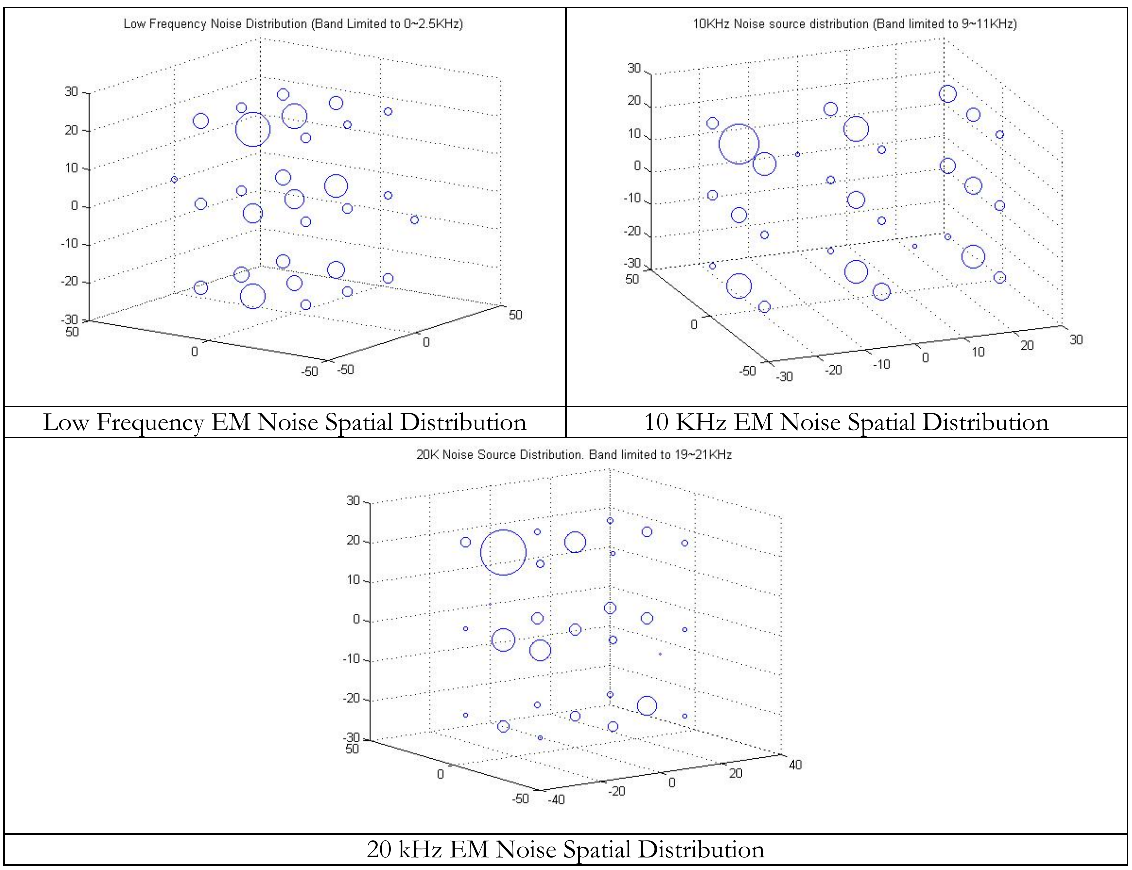

Low Frequency EM Noise Spatial Distribution

10 KHz EM Noise Spatial Distribution

20 kHz EM Noise Spatial Distribution

Figure 3.18 Spatial Distribution of EM Noise on Different Frequency Bands. The diameters of the circles show the integrated value of the power of noise over the frequency range of interest. The coordinates indicate the spatial position of the data points within the experimental volume.

In Figure 3.18, the center plane shows higher noise level comparing with front/back plane, indicating that the noise source mainly affects the image plane and attenuates quickly when getting further away from the center. Points close to the bore side get higher noise power which could also be interpreted as the effect of getting close to the noise source. Figures 3.19-22 show the time domain waveform on the solenoid when X-ray is working which are organized in accordance to the spatial order of test points in Figure 3. 15. The center plane is showing a higher noise power and clear X-ray working pulses appear in most of the charts while some peripheral points didn't show the X-ray working pulses which can be covered by a large amplitude lower frequency variation. Although X-ray pulses were evident in the front and back plane measurements, they were of lower amplitude than the imaging plane. No X-ray generation related pulses were evident for measurements made outside the bore.

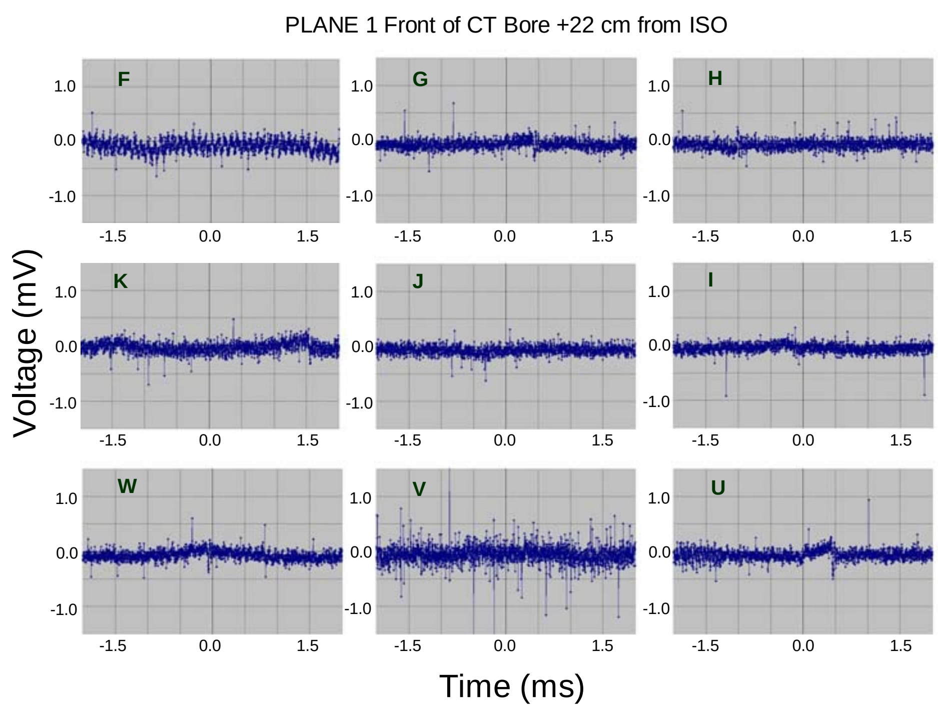

Figure 3.19 Purple Plane: Front of CT Bore, +22 cm from Isocenter

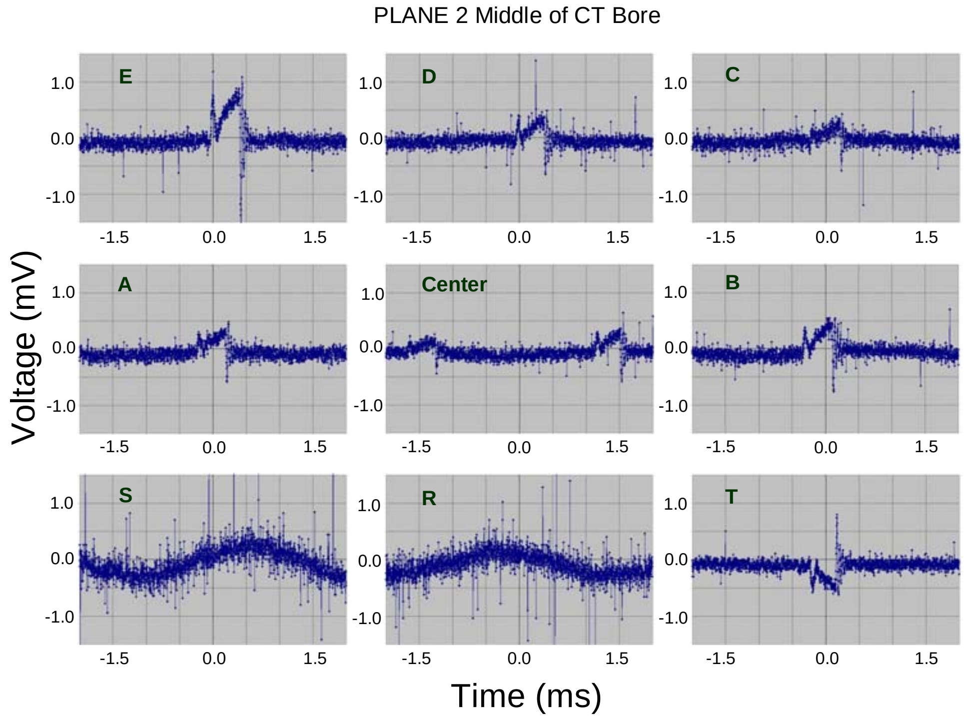

Figure 3.20 Green Plane: Middle of CT Bore

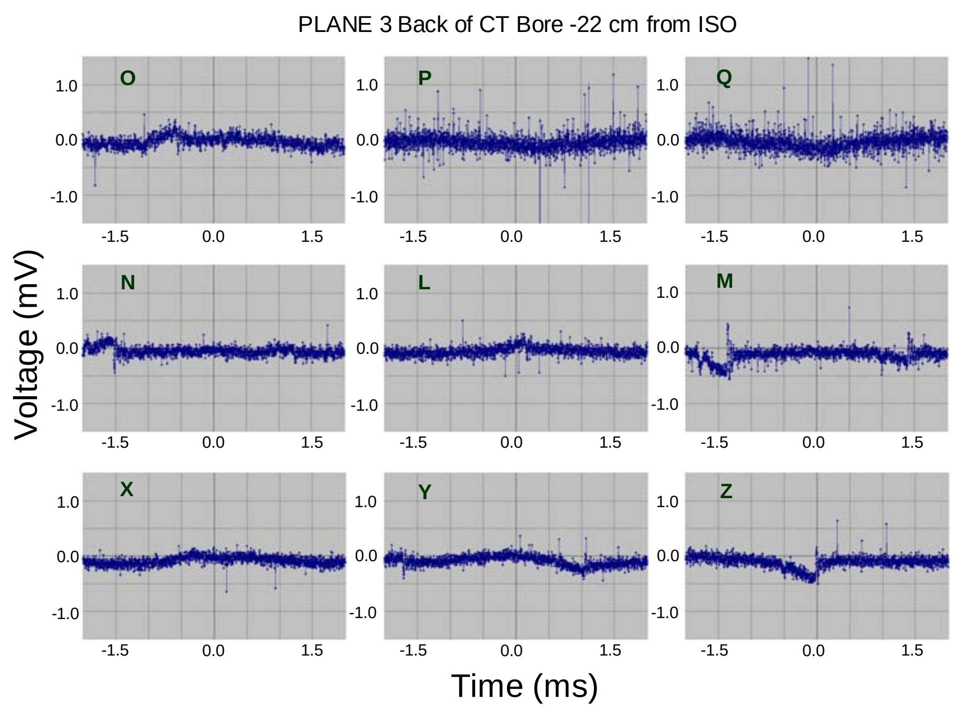

Figure 3.21 Orange Plane: Back of CT Bore, -22CM from Isocenter

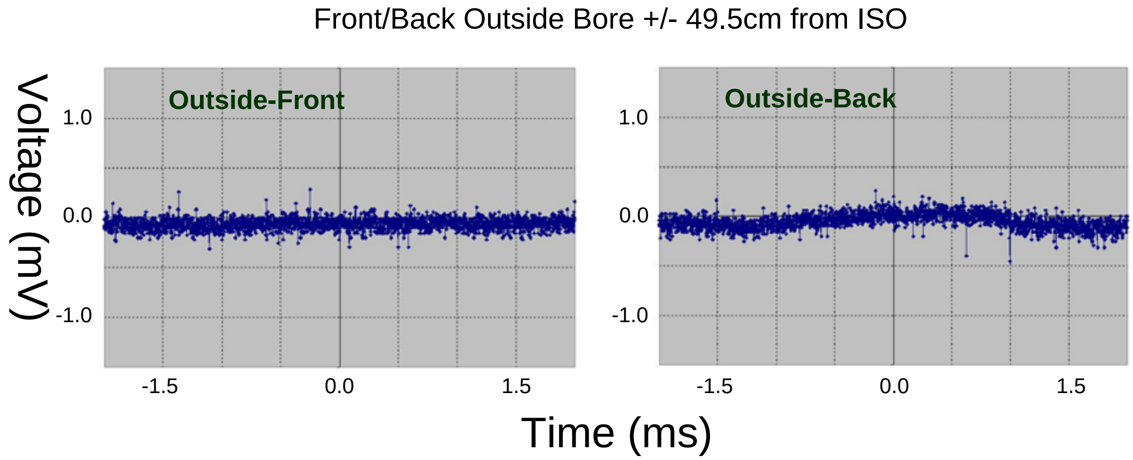

Figure 3.22 Outside CT Bore

Chapter 4

Conclusions and Future Work

4.1 Summary and Conclusions

This work describes the evaluation of the first wireless electromagnetic tracking system that performs tumor tracking concurrent with CT data acquisition in a CT environment. Current electromagnetic tracking systems require the operator to bring the patient outside of the CT bore before using the system, which adds delay between imaging and intervention, and also may lead to patient movement. Potential applications include using implanted transponders to guide imaging measurements of respiratory motion ('tumor correlated imaging' versus 'respiratory correlated imaging') as well as wireless tools for intervention procedures in the CT bore.

Experimental results showed a proper working volume of $14\times14\times14$ cm^3 inside the CT bore. With working parameters selected as sensor position close to the transponder and far from the CT gantry along with the front amplifier gain low on the Calypso system, the system can achieve the clinical goal of <2 mm RMS error. Experiment also excluded the possibility of using the high gain working mode which failed in all the tests by showing a high average noise power over the tracking volume generated by the rotating metal arm and other peripherals of the CT scanner. This kind of constant noise source cannot be canceled by using the gating method as used in LINAC environment.

4.2 Future Work

After evaluating the system under various working parameters the proper working conditions for the system in CT environment were established while quantified error measurements were acquired over the entire working volume. This dataset can also be used as a calibration tool.

Tests for studying system behavior while tracking a moving target will also be useful. All the tracking data sets acquired in this thesis are for stationary targets. However, when tracking a moving target there will be issues like tracking delay, sample rate and dynamic error rate. The Calypso system has shown to be accurate in the presence of motion in a linear accelerator environment, however a characterization study in the CT environment would be useful.

In the EM field characterization experiment, the noise showed an obvious location based pattern as well as frequency dependence. Additionally, EM characterization experiments can be conducted for error compensation, although this is potentially CT scanner specific.

Appendix A

Statistical Formulae

RMS:

$$RMS_{(x,y,z)} = \sqrt{\frac{1}{3}(x^2 + y^2 + z^2)}$$

The root mean square error, $e_{(x,y,z)}$ is evaluated as the mean square root of the values along each individual axis.

Variance:

$$\sigma^2 = \frac{1}{N}\sum_{i=1}^{N}(x_i - \bar{x})^2$$

Standard Deviation:

$$\sigma = \sqrt{\frac{1}{N}\sum_{i=1}^{N}(x_i - \bar{x})^2}$$

For standard deviation (σ) and variance (σ^2), N denotes the number of samples, and x_i, $\bar{x}$ denote the sample and mean, respectively. In this case, the standard deviation is for the samples concerned and variance is a bias-corrected sample variance.

Appendix B

Supplementary Data

CT	Rotation	Beacon to array	Array to bore	Gain	Orientation	Std1	Std2	Std3
off	-	20cm	14cm	high	y	0.12	0.12	0.13
off	-	20cm	14cm	high	z	0.09	0.1	0.08
off	1.5s	20cm	14cm	high	z	0.26	0.19	0.23
off	1.5s	20cm	14cm	high	z	0.29	0.21	0.19
on	1.5s	20cm	14cm	high	z	0.44	0.54	1.07
on	0.44s	20cm	14cm	high	z	2.5	1.4	3.4
off	AP (0)	20cm	26.5cm	high	z	0.096	0.091	0.11
on	0.44s	20cm	26.5cm	high	z	0.32	0.38	0.98
off	0.44s	20cm	26.5cm	high	z	0.12	0.12	0.15
on	0.44s	20cm	26.5cm	low	z	0.17	0.15	0.22
off	0.44s	20cm	26.5cm	low	z	0.16	0.17	0.21
off	AP (0)	20.5cm	14cm	low	z	0.2	0.23	0.25
off	0.44s	20.5cm	14cm	low	z	0.32	0.22	0.31
on	0.44s	20.5cm	14cm	low	z	0.37	0.27	0.37
off	AP (0)	20.5cm	14cm	low	y	0.12	0.098	0.07
off	0.44s	20.5cm	14cm	low	y	0.18	0.12	0.12
on	0.44s	20.5cm	14cm	low	y	0.18	0.14	0.11

CT	**Rotation time**	**Beacon to array**	**Array to bore**	**Gain**	**Phantom**	**Array Arm**
on	0.44s	20cm	14cm	low	y orientation	disconnected
off	0.44s	20cm	14cm	low	y orientation	disconnected
off	AP (0)	20cm	14cm	low	y orientation	disconnected
off (Outside Bore)	-	20cm	14cm	low	y orientation	disconnected
off (Outside Bore)	-	20cm	14cm	low	z orientation	disconnected
on	0.44s	20cm	14cm	low	z orientation	disconnected
off	0.44s	20cm	14cm	low	z orientation	disconnected
off	AP (0)	20cm	14cm	low	z orientation	disconnected
off(Outside Bore)	AP (0)	20cm	14cm	low	z orientation	disconnected
off (Outside Bore round 1)	-	20cm	26cm	low	z orientation	disconnected
on	0.44s	20cm	26cm	low	z orientation	disconnected
off	0.44s	20cm	26cm	low	z orientation	disconnected
off	AP (0)	20cm	26cm	low	z orientation	disconnected
outside2	AP (0)	20cm	26cm	low	z orientation	disconnected
on	0.44s	20cm	26cm	low	z orientation	disconnected
off	0.44s	20cm	26cm	low	z orientation	disconnected
off	AP (0)	20cm	26cm	low	z orientation	disconnected
on	0.44s	20cm	26cm	low	z orientation	disconnected
off	0.44s	20cm	26cm	low	z orientation	disconnected
off	AP (0)	20cm	26cm	low	z orientation	disconnected
off (Outside Bore)	-	20cm	26cm	low	z orientation	disconnected
off (Outside Bore Round 2)	-	20cm	26cm	low	y orientation	disconnected
on	0.44s	20cm	26cm	low	y orientation	disconnected
off	AP (0)	20cm	26cm	low	y orientation	disconnected
off	0.44s	20cm	26cm	low	y orientation	disconnected
off (Outside Bore Round 2)	-	20cm	26cm	low	y orientation	disconnected
off (Outside Bore Round 2)	-	20cm	26cm	low	y orientation	disconnected
on	0.44s	20cm	26cm	low	y orientation	disconnected
off	AP (0)	20cm	26cm	low	y orientation	disconnected
off	0.44s	20cm	26cm	low	y orientation	disconnected
off (Outside Bore Round 2)	-	20cm	26cm	low	y orientation	disconnected

Array offset	Beacon Offset	Std1	Std2	Std3	B1x	B1y	B1z	B2x	B2y	B2z	B3x	B3y	B3z
0	0	0.16	0.14	0.12	-0.45	-0.49	19.99	-0.95	0.02	19.98	0.06	0.38	19.95
0	0	0.12	0.13	0.12	-0.45	-0.5	19.94	-0.95	0.15	19.98	0.06	0.39	19.96
0	0	0.1	0.11	0.08	-0.45	-0.5	19.92	-0.95	-0.01	19.93	0.05	0.37	19.92
0	0	0.08	0.1	0.08	-0.44	-0.5	19.93	-0.94	-0.02	19.94	0.05	0.36	19.93
0	0	0.12	0.12	0.15	-0.27	2	20.27	0.97	-0.1	20.29	-1.49	-0.11	20.26
0	0	0.31	0.21	0.27	-0.24	1.98	20.3	0.97	-0.14	20.4	-1.5	-0.16	20.36
0	0	0.26	0.23	0.26	-0.25	2.02	20.36	0.98	-0.13	20.41	-1.54	-0.12	20.34
0	0	0.16	0.16	0.2	-0.31	2.09	20.24	0.89	-0.1	20.25	-1.5	-0.11	20.22
0	0	0.12	0.12	0.15	-0.28	2.02	20.27	0.97	-0.09	20.29	-1.47	-0.12	20.28
0	0	0.13	0.11	0.14	-0.28	2.03	20.32	0.98	-0.11	20.32	-1.47	-0.11	20.29
0	0	0.17	0.15	0.18	-0.27	2.03	20.32	0.96	-0.11	20.34	-1.49	-0.1	20.31
0	0	0.14	0.14	0.19	-0.27	2.06	20.33	0.97	-0.08	20.24	-1.51	-0.09	20.31
0	0	0.13	0.12	0.16	-0.26	2.06	20.29	0.97	-0.06	20.32	-1.5	-0.1	20.31
0	0	0.13	0.12	0.15	-0.26	2.04	20.3	0.96	-0.1	20.31	-1.46	-0.11	20.28
3.5	0	0.17	0.13	0.2	-0.13	2.21	20.32	1.05	0.05	20.33	-1.4	0.09	20.29
3.5	0	0.15	0.13	0.17	-0.16	2.25	20.33	1.06	0.06	20.32	-1.4	0.12	20.31
3.5	0	0.11	0.12	0.17	-0.12	2.22	20.27	1.06	0.07	20.34	-1.4	0.1	20.3
3.5	6-7cm	0.16	0.19	0.19	5.68	2.15	20.34	6.97	-0.01	20.36	4.44	0.02	20.37
3.5	6-7cm	0.17	0.21	0.23	5.67	2.15	20.34	6.99	0	20.36	4.48	0.01	20.39
3.5	6-7cm	0.11	0.18	0.15	5.63	2.16	20.31	6.97	0	20.35	4.42	0.04	20.34
3.6	6-7cm	0.12	0.15	0.17	5.64	2.13	20.34	6.94	0.02	20.35	4.44	0.01	20.36
3.5	6-7cm	0.11	0.12	0.11	6.56	2.51	20.2	6.04	2.99	20.23	7.03	3.41	20.22
3.5	6-7cm	0.17	0.16	0.18	6.56	2.52	20.13	6.05	3	20.23	7.03	3.4	20.21
3.5	6-7cm	0.14	0.12	0.11	6.56	2.51	20.13	6.06	3	20.24	7.03	3.41	20.19
3.6	6-7cm	0.15	0.17	0.14	6.56	2.52	20.18	6.06	2.99	20.23	7.03	3.41	20.22
3.5	6-7cm	0.13	0.13	0.12	6.56	2.5	20.2	6.05	2.98	20.26	7.02	3.4	20.2
0	0	0.1	0.12	0.08	-0.47	-0.25	20.19	-0.98	0.23	20.26	0	0.64	20.25
0	0	0.12	0.12	0.09	-0.48	-0.23	20.22	-1	0.24	20.26	-0.01	0.65	20.24
0	0	0.09	0.1	0.08	-0.48	-0.24	20.2	-0.99	0.24	20.25	0	0.65	20.23
0	0	0.1	0.12	0.11	-0.48	-0.24	20.19	-0.98	0.24	20.24	-0.01	0.65	20.22
0	0	0.09	0.11	0.09	-0.47	-0.25	20.18	-0.99	0.23	20.26	-0.01	0.65	20.24

References

[1] Z. Yaniva, E. Wilson, D. Lindisch and K. Cleary, "Electromagnetic tracking in the clinical environment," Med. Phys. **36**, 876-892 (2009).

[2] S. Marnitz, M. Stuschke, J. Bohsung, *et al.*, "Intraindividual comparison of conventional three-dimensional radiotherapy and intensity modulated radiotherapy in the therapy of locally advanced non-small cell lung cancer," Strahlenther Onkol **178**, 651-658 (2002).

[3] E. A. Barnes, B. R. Murray, D. M. Robinson, *et al.* "Dosimetric evaluation of lung tumor immobilization using breath hold at deep inspiration," Int J Radiat Oncol Biol Phys **50,** 1091-1098 (2001).

[4] V. V. Kindratenko, "A survey of electromagnetic position tracker calibration techniques," Virtual Reality: Research, Development and Applications **5**, 169-182 (2000).

[5] W. Smith, I. Vesely, A. Gubbels, "Three-Dimensional Digital Ultrasound Tracking System" US Patent, 5,515,853.

[6] W. Smith and I. Vesely, "Three dimensional ultrasonic micrometer in use for cardiovascular research," IEEE in Medicine and Biology Society **13**, 1520-1521 (1994).

[7] M. A. Nixon, B. C. McCallum, W. R Fright and N. B. Price, "The Effects of Metals and Interfering Fields on Electromagnetic Trackers," Presence **7**, 204-218 (1998).

[8] S. Ramo, J.R. Whinnery, T. Duzer, "Fields and Waves in Communication Electronics," New York and London: John Wiley, 122-125 (1965)

[9] H. Shirato, S. Shimizu, T. Kunieda, *et al.*, "Physical Aspects of a Real-time Tumor-Tracking System for Gated Radiotherapy," Int J Radiat Oncol Bio Phy, **48**:1187-1195 (2000).

[10] J. Hummel, M. Figl, C. Kollmann and H. Bergmann, "Evaluation of a Miniature Electromagnetic Position Tracker," Med. Phys. **29**, 2205-2212 (2002).

[11] R. L. Smith, A. Sawant, L. Santanam, *et al.*, "Integration of Real-Time Internal Electromagnetic Position Monitoring Coupled with Dynamic Multileaf Collimator Tracking: An IMRT Feasibility Study," Int J Radiat Oncol Bio Phy, **74,** 868-875 (2009).

[12] A. Sawant, R. L. Smith, R. B. Venkat, *et al.*, "Toward Submillimeter Accuracy in the Management of Intrafraction Motion: The Integration of Real-Time Internal Position Monitoring and Multileaf Collimator Target Tracking," Int. J. Radiation Oncology Biol. Phys. **74**, 575-582 (2009).

[13] R. L. Smith, K. Lechleiter, K. Malinowski, *et al.*, "Evaluation of LINAC Gating With Real-Time Electromagnetic Tracking," Int J Radiat Oncol Bio Phy, **74**:920-927 (2009).

[14] F. Raab, E. Blood, T. Steiner and R. Jones, "Magnetic position and orientation tracking system," IEEE Trans. AES **15**, 709-718 (1979).

[15] M. A. Livingston and A. State, "Magnetic tracker calibration for improved augmented reality registration," Presence **6**, 532-546 (1997).

[16] A. M. Balter and J. N. Wright, "Accuracy of a wireless localization system for radiotherapy," Int. J. Radiation Oncology Biol. Phys. **61**, 933-937 (2005).

[17] F. Banovac, J. Tang, S. Xu, *et al.*, "Precision targeting of liver lesions using a novel electromagnetic navigation device in physiologic phantom and swine," Med. Phys. **32**, 2698-2705 (2005).

[18] F. Banovac, N. Glossop, D. Lindisch, *et al.*, "Liver Tumor Biopsy in a Respiring Phantom With the Assistance of a Novel Electromagnetic Navigation Device," MICCAI, LNCS 2488: 200-207 (2002).

[19] J. Hummel, C. M. Jun, M. Figl, *et al.*, "Standardized Evaluation Method for Electromagnetic Tracking Systems," Proc. SPIE **5744**, 236-240 (2005).

[20] D. C. Barratt, A. H. Davies, A. D. Hughes, *et al.*, "Accuracy of an electromagnetic Three-Dimensional Ultrasound System for Carotid Artery Imaging," Ultrasound Med Biol. **27**, 1421-1425 (2001).

[21] A. J. Chung, P. J. Edwards, F Deligianni and G. Z. Yang, "Freehand Cocalibration of Optical and Electromagnetic Trackers for Navigated Bronchoscopy," MIAR, LNCS 3150: 320-328 (2004).

[22] W. D. Curtis, A. L. Janin and K. Zikan, "A note on averaging rotations," in Virtual Reality Annual International Symposium, pp. 377-385 (1993).

[23] F. J. Ferrin, "Survey of Helmet Tracking Technologies," Proc. SPIE **1456**, 86-94 (1991).

[24] J. M. Fitzpatrick, J. B. West and C. R. Maurer, "Predicting Error in Rigid-Body Point-Based Registration," IEEE Trans. in Med. Imaging **17**, 694-702 (1998).

[25] J. M. Fitzpatrick, P. E. Konrad, C. Nickele, E. Cetinkaya and C. Kao "Accuracy of Customized Miniature Stereotactic Platforms," Stereotactic Functional Neurosurgery **83**, 25-31 (2005).

[26] D. D. Frantz, A. D. Wiles, S. E. Leis and S. R. Kirsch, "Accuracy Assessment Protocols for Electromagnetic Tracking Systems," Phys. Med. Biol. **48**, 2241- 2251 (2003).

[27] E. Wilson, "Accuracy Analysis of Electromagnetic Tracking within Medical Environments," M. S. Dissertation, Georgetown University, Washington, DC (2006).

[28] D. R. Gauldie, "Calibration and Registration With 3D A-Mode Ultrasound," MSc Dissertation, Queen's University, Kingston, Ontario, Canada (2002).

[29] B. K. P. Horn, H. M. Hilden, and S Negahdaripour, "Closed-Form Solution of Absolute Orientation Using Orthonormal Matrices," J. Opt. Soc. Am. A **5**, 1127-1135 (1988).

[30] B. K. P. Horn, "Closed-form Solution of Absolute Orientation Using Unit Quaternions," J. Opt. Soc. Am. A **4**, 629-642 (1987).

[31] J. Hummel, M. R. Bax, M. L. Figl, *et al.*, "Design and Application of an Assessment Protocol for Electromagnetic Tracking Systems," Med. Phys. **32**, 2371-2378 (2005).

[32] M. Ikits, J. D. Brederson, C. D. Hansen and J. M. Hollerbach, "An Improved

Calibration Framework for Electromagnetic Tracking Devices," Proc. IEEE, Virtual Reality, pp. 63-70 (2001).

[33] V. V. Kindratenko and A. Bennett, "Evaluation of rotation correction techniques for electromagnetic position tracking systems," Virtual Environments: Proceedings of the Eurographics Workshop, pp. 13-22 (2000).

[34] J. B. A. Maintz and M. A. Viergever, "A Survey of Medical Image Registration," Medical Image Analysis **2**, 1-36 (1998).

[35] K. Nakada, M. Nakamoto, Y. Sato, *et al.*, "A Rapid Method for Magnetic Tracker Calibration Using a Magneto-Optic Hybrid Tracker," MICCAI, LNCS 2879: 285-293 (2003).

[36] K. Schicho, M. Figl, M. Donat, W. Brickfellner, *et al.*, "Stability of Miniature Electromagnetic Tracking Systems," Phys. Med. Biol. **50**, 2089-2098 (2005).

[37] A. Schweikard, H. Shiomi and J. Adler, "Respiration tracking in radiosurgery without fiducials," Int J Med. Robotics and Computer Assisted Surgery **1**, 19-27 (2005).

[38] P. G. Seiler, H. Blattmann, S. Kirsch, R. K. Muench and C. Schilling, "A Novel Tracking Technique for the Continuous Precise Measurement of Tumour Position in Conformal Radiotherapy," Phys. Med. Biol. **45**: N103-N110 (2000).

[39] B. M. Stoeckelhuber, E. Schulz, U. H Melchert, *et al.*, "Procedures, spectrum and radiation exposure in CT-fluoroscopy," Rontgenpraxis **55**, 51-57 (2003).

[40] R. Taylor, P. Jensen, L. Whitcomb, A. Barnes, R. Kumar, D. Stoianovici, *et al.*, "A

Steady-Hand Robotic System for Microsurgical Augmentation," Intl Journal of Robotics Research December **18**, 1201-1210 (1999).

[41] S. Umeyama, "Least-Squares Estimation of Transformation Parameters Between Two Point Patterns," IEEE Trans. on Pattern Analysis and Machine Intelligence **13**, 376-380 (1991).

[42] B. J. Wood, H. Zhang, A. Durrani, *et al.*, "Navigation with electromagnetic tracking for interventional radiology procedures: A feasibility study," J Vasc Interv Radiology **16**, 493-505 (2005).

[43] X. Wu and R. Taylor, "A Direction Space Interpolation Technique for Calibration of Electromagnetic Surgical Navigation Systems," MICCAI, LNCS 2879: 215-222 (2003).

[44] G. Zachmann, "Distortion correction for magnetic fields for position tracking," IEEE Intl. Conference on Computer Graphics, pp. 213-220 (1997).

[45] P. J. Parikh, K. M. Lechleiter, K. L. Malinowskai, R. L. Smith, J. Wen, and S. Dimmer, "Tumor correlated CT: A new paradigm for motion compensated CT for image guided-therapy," Proc. SPIE **7261**, 726121-726121-8 (2009).

[46] C. Nafisa, V. Jensenb, L. Beauregardc and P. Andersonc, "Method for estimating dynamic EM tracking accuracy of Surgical Navigation tools," Proc. SPIE **6141**, 152-167 (2006).

[47] J. Hanley, M. M. Debois, D. Mah, *et al.*, "Deep inspiration breathhold technique for lung tumors: The potential value of target immobilization and reduced lung density in

dose escalation," Int J Radiat Oncol Biol Phys **45,** 603-611 (1999).

[48] K. E. Rosenzweig, J. Hanley, D. Mah, *et al.*, "The deep inspiration breath-hold technique in the treatment of inoperable nonsmall-cell lung cancer," Int J Radiat Oncol Biol Phys **48**, 81-87 (2000).

[49] G. S. Margeras, E. Yorke, "Deep inspiration breath hold and respiratory gating strategies for reducing organ motion in radiation treatment," Semin Radiat Oncol **14,** 65-75 (2004).

[50] N. Koch, H. H. Liu, G. Starkschall, *et al.*, "Evaluation of internal lung motion for respiratory-gated radiotherapy using MRI: Part I—Correlating internal lung motion with skin fiducial motion," Int J Radiat Oncol Biol Phys **60,** 1459-1472 (2004).

[51] R. I. Berbeco, S. Nishioka, H. Shirato, *et al.*, "Residual motion of lung tumors in gated radiotherapy with external respiratory surrogates," Phys Med Biol **50,** 3655-3667(2005).

[52] C. Ozhasoglu, M. J. Murphy, "Issues in respiratory motion compensation during external-beam radiotherapy," Int J Radiat Oncol Biol Phys **52,** 1389-1399 (2002).

[53] Varian Medical, [HTML] Available: http://www.varian.com

[54] Immersion Company, [HTML] Available: http://www.emicroscribe.com

[55] Polhemus Company, [HTML] Available: http://www.polhemus.com

[56] Ascension Technology Corp., [HTML] Available: http://ascension-tech.com

[57] Northern Digital Inc., [HTML] Available: http://www.ndigital.com

[58] Calypso Medical, [HTML] Available: http://www.calypsomedical.com

[59] Philips Medical, [HTML] Available: http://www.medical.philips.com

[60] WIKIPEDIA, [HTML] Available: http://www.wiki.org

Vita

Jie Wen

Date of Birth	Jan 19, 1984		
Place of Birth	Shanghai, China		
Degrees	B. S.	Electrical Engineering Shanghai Jiaotong University, Shanghai, China	July 2006

Publications

Parag J Parikha, Kristen M Lechleitera, Kathleen L Malinowskai, Ryan L. Smitha, Jie Wen, Steve Dimmerb, " Tumor correlated CT: A new paradigm for motion compensated CT for image guided-therapy," Proc. SPIE, **7261**, 726121 (2009)

P Parikh, J Wen, R Smith, C Noel, L Santanam, J Petersen, J Newell, S Dimmer, "Concurrent wireless electromagnetic tracking and CT imaging," Med. Phys. **36**, Issue 6 (2009)

P. K. Yalavarthy, Z. Wei, J. Wen, P. Parikh, T. Zhao, J. Bradely, D. Low, "A Spatially-based Binning Method for Improving the Quantitative Accuracy of Free-breathing PET/CT Images," International J. Radiation Oncology Biol. Phys., **72**, Issue 1(2008)

May 2010

EM Tracking Device Study,   Wen, M.S. 2010